therapy with cytostatic agents targeting at DNA-topoisomerase II. *Blood* 1991;**78**:1147–8.
32. Soenen V, Preudhomme C, Roumier C, Daudignon A, Lai JL, Fenaux P. 17p Deletion in acute myeloid leukemia and myelodysplastic syndrome. Analysis of breakpoints and deleted segments by fluorescence in situ. *Blood* 1998;**91**:1008–15.
33. Merlat A, Lai JL, Sterkers Y, Demory JL, Bauters F, Preudhomme C, Fenaux P. Therapy-related myelodysplastic syndrome and acute myeloid leukemia with 17p deletion. A report on 25 cases. *Leukemia* 1999;**13**:250–7.
34. Sessarego M, Ajmar F. Correlation between acquired pseudo-Pelger-Huet anomaly and involvement of chromosome 17 in chronic myeloid leukemia. *Cancer Genet Cytogenet* 1987;**25**:265–70.
35. Ahuja H, Bar-Eli M, Arlin Z, Advani S, Allen SL, Goldman J, Snyder D, Foti A, Cline M. The spectrum of molecular alterations in the evolution of chronic myelocytic leukemia. *J Clin Invest* 1991;**87**:2042–7.
36. Vardiman JW, Harris NL, Brunning RD. The World Health Organization (WHO) classification of the myeloid neoplasms. *Blood* 2002;**100**:2292–302.
37. Wandt H, Schakel U, Kroschinsky F, Prange-Krex G, Mohr B, Thiede C, Pascheberg U, Soucek S, Schaich M, Ehninger G. MLD according to the WHO classification in AML has no correlation with age and no independent prognostic relevance as analyzed in 1766 patients. *Blood* 2008;**111**:1855–61.

Down-regulation of CD20 expression in B-cell lymphoma cells after treatment with rituximab-containing combination chemotherapies: its prevalence and clinical significance

Junji Hiraga,[1,2] Akihiro Tomita,[1] Takumi Sugimoto,[1] Kazuyuki Shimada,[1] Masafumi Ito,[3] Shigeo Nakamura,[4] Hitoshi Kiyoi,[5] Tomohiro Kinoshita,[1] and Tomoki Naoe[1]

[1]Department of Hematology and Oncology, Nagoya University Graduate School of Medicine, Nagoya; [2]Department of Hematology, Toyota Memorial Hospital, Toyota; [3]Department of Pathology, Japanese Red Cross, Nagoya First Hospital, Nagoya; [4]Department of Pathology and Clinical Laboratories, Nagoya University Hospital, Nagoya; and [5]Department of Infectious Diseases, Nagoya University School of Medicine, Nagoya, Japan

Although rituximab is a key molecular targeting drug for CD20-positive B-cell lymphomas, resistance to rituximab has recently been recognized as a considerable problem. Here, we report that a CD20-negative phenotypic change after chemotherapies with rituximab occurs in a certain number of CD20-positive B-cell lymphoma patients. For 5 years, 124 patients with B-cell malignancies were treated with rituximab-containing chemotherapies in Nagoya University Hospital. Relapse or progression was confirmed in 36 patients (29.0%), and a rebiopsy was performed in 19 patients. Of those 19, 5 (26.3%; diffuse large B-cell lymphoma [DLBCL], 3 cases; DLBCL transformed from follicular lymphoma, 2 cases) indicated CD20 protein-negative transformation. Despite salvage chemotherapies without rituximab, all 5 patients died within 1 year of the CD20-negative transformation. Quantitative reverse-transcription–polymerase chain reaction (RT-PCR) showed that CD20 mRNA expression was significantly lower in CD20-negative cells than in CD20-positive cells obtained from the same patient. Interestingly, when CD20-negative cells were treated with 5-aza-2′-deoxycytidine in vitro, the expression of CD20 mRNA was stimulated within 3 days, resulting in the restoration of both cell surface expression of the CD20 protein and rituximab sensitivity. These findings suggest that some epigenetic mechanisms may be partly related to the down-regulation of CD20 expression after rituximab treatment. (Blood. 2009;113: 4885-4893)

Introduction

Rituximab is a murine/human chimeric anti-CD20 monoclonal antibody that has become a key molecular targeting drug for CD20-positive B-cell lymphomas.[1,2] Many favorable results using combination chemotherapy with rituximab for both CD20-positive de novo and relapsed low-grade and aggressive B-cell non-Hodgkin lymphoma have been reported in recent years.[3-7] In Japan, rituximab has also been used since September 2001 for patients with follicular lymphoma (FL), indolent lymphoma, and mantle cell lymphoma (MCL). In addition, since September 2003 in Japan, indications for using rituximab were expanded to include diffuse large B-cell lymphoma (DLBCL), further demonstrating the significant effectiveness of rituximab for B-cell lymphoma compared with conventional chemotherapies without rituximab.[8]

Although combination chemotherapies with rituximab have provided significantly favorable results for CD20-positive B-cell lymphoma patients, acquired resistance to rituximab has become a considerable problem. Several mechanisms of resistance were predicted as reported previously, including loss of CD20 expression, inhibition of antibody binding, antibody metabolism, expression of complement inhibitors such as CD55/CD59, and membrane/lipid raft abnormality (reviewed by Smith et al[9]),[10-19] but the clinical significance of those mechanisms has remained unclear. In the last 5 years, a CD20-negative phenotypic change in CD20-positive lymphomas after rituximab treatment has been reported by several groups,[16,20-31] indicating that this phenomenon after the use of rituximab may not be rare. Although these reports contain important information from clinical experiences, the frequency of occurrence and detailed molecular biologic information about the CD20-negative phenotype remain to be elucidated.

Very recently, we reported a CD20-negative DLBCL case that had transformed from CD20-positive FL after repeated treatment with rituximab. We established an RRBL1 cell line from this patient,[32] and the mechanisms of the CD20-negative change were analyzed in these cells. CD20 mRNA expression was significantly lower than in CD20-positive cells, resulting in a loss of CD20 protein expression as detected by flow cytometry (FCM), immunohistochemistry (IHC), and immunoblotting (IB). Interestingly, trichostatin A (TSA), a histone deacetylase inhibitor, was able to successfully stimulate CD20 expression, suggesting that some epigenetic mechanisms may have repressed the expression. Thus, an accumulation of detailed clinical and molecular biologic features is required to demonstrate the significance of CD20-negative phenotypic changes after rituximab treatment.

In the last 5 years, 124 patients with CD20-positive B-cell malignancies received chemotherapy with rituximab at Nagoya University Hospital, 36 (29.0%) of whom showed relapse/progression. Among these 36 patients, CD20 protein-negative or -decreased phenotypic changes were confirmed in 5 cases concomitant with disease progression. Here, we describe the occurrence rate of CD20-negative transformation after rituximab treatment, as well

Submitted August 19, 2008; accepted February 25, 2009. Prepublished online as *Blood* First Edition paper, February 26, 2009; DOI 10.1182/blood-2008-08-175208.

The online version of this article contains a data supplement.

The publication costs of this article were defrayed in part by page charge payment. Therefore, and solely to indicate this fact, this article is hereby marked "advertisement" in accordance with 18 USC section 1734.

Table 1. CD20-positive B-cell malignancies treated with rituximab in Nagoya University Hospital

	No. of patients	Disease status at rituximab therapy		Response, RD/PD	Resampling of tumor tissue	CD20 expression, +/±/−
		1st	RD/PD			
DLBCL	51	45	6	13	6	3/1/2
FL	43	26	17	13	7	5/0/2
Nodal marginal zone BCL or MALT	8	6	2	2	2	2/0/0
Burkitt or Burkitt-like	5	5	0	4	2	2/0/0
Mediastinal large B-cell	4	2	2	1	0	0
Intravascular large B-cell	4	4	0	2	1	1/0/0
Mantle cell	4	3	1	1	1	1/0/0
Lymphoplasmacytic	3	3	0	0	0	0
CLL/SLL	2	1	1	0	0	0
Total cases	124	96	28	36	19	14/1/4
Probability (%)				36/124 (29.0)	19/36 (52.5)	5/19 (26.3)

DLBCL indicates diffuse large B-cell lymphoma; FL, follicular lymphoma; BCL, B-cell lymphoma; MALT, mucosa-associated lymphoid tissue; CLL/SLL, clonic lymphocytic leukemia/small lymphocytic lymphoma; 1st, the first treatment; RD/PD, relapse or progression; and +/±/−; positive/decreased/negative.

as the molecular background of the CD20 protein-negative phenotype in cells from those patients.

Methods

Patients

Between February 1988 and November 2006 in Nagoya University Hospital, all 124 patients in this analysis were initially diagnosed with CD20-positive B-cell lymphomas (Table 1) according to the World Health Organization (WHO) classification.[33] All patients were treated with combination chemotherapy with rituximab from September 2001 to December 2006. The median age of the patients was 58 years (range, 16-84 years) at the time of initial rituximab administration. Three patients had received rituximab before September 2001 because of their participation in a previous clinical study. The most recent follow-up date was July 31, 2007, and disease status factors such as relapse, recurrence, and progression were determined by clinical findings and diagnostic imaging using x-ray, computed tomography (CT), magnetic resonance imaging (MRI), and ^{18}F-fluorodeoxyglucose positron emission tomography (FDG-PET). Resampling of tumors at the time of relapse/progression and pathologic analysis of 19 patients was performed. The patients' responses to chemotherapies were evaluated using the International Working Group criteria.[34]

Confirmation of CD20 protein expression by IHC and FCM analyses

These studies were conducted with institutional review board approval from the Nagoya University School of Medicine. After obtaining appropriate informed consent from each patient, in accordance with the Declaration of Helsinki, tumor specimens were harvested from lymph nodes, bone marrow, peripheral blood, or spinal fluid. CD20 protein expression was demonstrated by IHC and/or FCM as indicated previously.[32,35] Briefly, we used mouse anti-CD20 (L26; Dako, Carpinteria, CA), anti-CD10 (Novocastra Laboratories, Newcastle-upon-Tyne, United Kingdom), and anti-CD79a monoclonal antibodies (Dako) for IHC, and mouse anti-CD20 (B2E9; Beckman Coulter, Fullerton, CA) and anti-CD19 (HD37; Dako) monoclonal antibodies for FCM. The CD79a antigen is a pan–B-cell marker that forms a B-cell receptor (BCR) protein complex. The percentages of negative and positive cells from FCM were determined from the data using an isotypic control antibody (mouse IgG1; Beckman Coulter).

Sequence analysis of the *MS4A1* (*CD20*) gene

Genomic DNA from tumor cells was extracted with a QIAamp DNA Blood Mini Kit (QIAGEN, Valencia, CA) and used for further polymerase chain reactions (PCRs). When sufficient tumor cells could not be obtained at diagnosis, genomic DNA from paraffin sections was extracted using the MagneSil Genomic, Fixed Tissue System (Promega, Madison, WI). Genomic DNA PCR was performed using AmpliTaq Gold (Applied Biosystems, Foster City, CA) to acquire fragments of the coding sequences of exons 3 to 8 of the *MS4A1* (*CD20*) gene. The following primers were designed from the appropriate intron sequences to achieve the coding sequences: exon 3-upper (U), 5′-GCT CTT CCT AAA CAA CCC CT-3′; exon 3-lower (L), 5′-CAT GGG ATG GAA GGC AAC TGA C-3′; exon 4-U, 5′-TGC TGC CTC TGT TCT CTC CC-3′; exon 4-L, 5′-CTG CAC CAT TTC CCA AAT GGC T-3′; exon 5-U, 5′-CTC CAT CTC CCC CAC CTC TC-3′; exon 5-L, 5′-GGT ACT TCT CTG ACA TGT GGG A-3′; exon 6-U, 5′-TGG AAT TCC CTC CCA GAT TAT G-3′; exon 6-L, 5′-CCT GGA GAG AAA TCC AAT CTC A-3′; exon 7-U, 5′-GTC TCC TGT ACT AGC AGT TC-3′; exon 7-L, GGC TAC TAC TTA CAG ATT TGG G-3′; exon 8-U, 5′-TGG TCA ATG TCT GCT GCC CT-3′; and exon 8-L, 5′-GCG TAT GTG CAG AGT ACC TCA AG-3′. Amplified fragments were cloned into a pGEM-T Easy Vector (Promega) and were sequenced using a DNA auto sequencer (ABI PRISM 310; Applied Biosystems). PCR fragments that contained each exon sequence were cloned into the pGEM-T vector, and at least 10 clones were sequenced. If a mutation was observed in 2 different clones, we verified that the sequence reflected a mutation in the tumor rather than a PCR error.

RNA extraction and reverse-transcription–polymerase chain reaction

A blood RNA extraction kit (QIAGEN) was used to isolate total RNA from tumor cells. cDNA was prepared as reported previously.[36] For reverse-transcription–polymerase chain reaction (RT-PCR) analyses of CD10, CD19, CD20, and β-actin, the following primers were designed: CD10-U, 5′-TTG TCC TGC TCC TCA CCA TC-3′; CD10-L, 5′-GTT CTC CAC CTC TGC TAT CA-3′; CD19-U, 5′-GAA GAG GGA GAT AAC GCT GT-3′; CD19-L, 5′-CTG CCC TCC ACA TTG ACT G-3′; CD20-U, 5′-ATG AAA GGC CCT ATT GCT ATG-3′; CD20-L, 5′-GCT GGT TCA CAG TTG TAT ATG-3′; β-actin-U, 5′-TCA CTC AAG ATC CTC A-3′; and β-actin-L, 5′-TTC GTG GAT GCC ACA GGA C-3′. Semiquantitative RT-PCR with AmpliTaq Gold was performed as described previously.[32] Quantitative RT-PCR was carried out using TaqMan PCR (ABI PRISM 7000; Applied Biosystems) as previously described.[32,36]

Immunoblot analysis

Cells (~5 × 10^5) were lysed in 100 μL lysis buffer (50 mM tris(hydroxymethyl)aminomethane [Tris]-HCl [pH 8.0], 1.5 mM $MgCl_2$, 1 mM ethylene glycol-bis(β-aminoethyl ester)-*N,N,N′,N′*-tetraacetic acid [EGTA], 5 mM KCl, 10% glycerol, 0.5% Nonidet P-40 [NP-40], 300 mM NaCl, 0.2 mM phenylmethylsulfonyl fluoride [PMSF], 1 mM dithiothreitol [DTT], and a Complete Mini protease inhibitor tablet [Roche Applied Science, Indianapolis, IN]). After centrifugation at 10 000*g* for 10 minutes, the supernatants were placed in new tubes and 100 μL of 2× sodium dodecyl sulfate (SDS) sample buffer was added. After boiling for 5 minutes, samples were

Table 2. CD20-negative RD/PD after treatment with rituximab-containing combination chemotherapy

UPN	Age/ sex	Diagnosis on admission	Status	Chemo Regimen	Total ritux	Duration until CD20−	Diagnosis (RD/PD)	Patho source	CD20 expression				Survival after CD20−
									FCM	IHC	RT	CDS mutation	
1	65/M	DLBCL	2 rel	R-salvage	8	2M	DLBCL	BM	−	−	N.A.	S97F [2/16]	6M†
2	37/ F	DLBCL	1 diag	R-CHOP	8	9M	DLBCL	BM	±*	±†	N.A.	V247I [2/10]	4M†
3	75/M	DLBCL	1 diag	R-CHOP	7	10M	DLBCL	BM, CF	−	−	↓	WT	11M†
4	42/M	FL G1	2 rel	R-CHOP	4	23M	DLBCL	BM	−	−	↓	WT	11M†
5	52/M	FL G2	3 rel	R-cMOPP	14	81M	DLBCL	BM, LN‡	−	−	↓	WT	8M†

Status indicates disease status of those patients at the first treatment with rituximab; rel, relapse; duration until CD20−, duration (in months) until CD20− relapse or PD from the first rituximab treatment; total ritux, total times of rituximab treatment; patho source, sources of tumor tissues for pathologic analysis; BM, bone marrow; CF, cerebral fluid; LN, lymph node; RT, RT-PCR; N.A., not available; ↓, down-regulated; CDS, coding sequences; and survival after CD20−, duration from CD20-negative change until death.

*19% of tumor cells were $CD20^+$.

†30% of tumor cells showed $CD20^+$.

‡Lymph node sample obtained at autopsy.

separated by SDS–polyacrylamide gel electrophoresis (PAGE). Immunoblotting was carried out as described previously[32,37] using goat polyclonal anti-CD20 antibody (Santa Cruz Biotechnology, Santa Cruz, CA) and rabbit polyclonal anti-actin antibody (Santa Cruz Biotechnology).

Treatment of RRBL1 cells and primary lymphoma cells with the epigenetic drug 5-aza-2′-deoxycytidine

RRBL1[32] and primary lymphoma cells (5×10^5) were cultured in 6-well dishes in RPMI 1640 medium containing 10% fetal bovine serum (FBS) for 24 hours with or without 5-aza-2′-deoxycytidine (5-Aza; Sigma-Aldrich, St Louis, MO) at a final concentration of 100 mM. The cells were then washed twice with RPMI 1640 medium containing 10% FBS, and incubated for more than 2 days in the same medium without 5-Aza. Cells were harvested and used for total RNA and protein extraction.

Antibody-dependent cell-mediated cytotoxicity assay in vitro

Antibody-dependent cell-mediated cytotoxicity (ADCC) activity was analyzed by an in vitro chromium-51 (^{51}Cr) release assay. Target cells (RRBL1, Daudi, DHL10) were cultured in appropriate medium supplemented with 10% to 20% FBS. Each cell line (2.0×10^5 cells) was labeled with 100 μCI (3.7 MBq) of $Na_2{}^{51}CrO_4$ (PerkinElmer Japan, Tokyo, Japan) at 37°C for 1 hour. Human peripheral blood mononuclear cells (PBMC), which were obtained from a healthy donor, were prepared as effector cells of the cell-mediated cytotoxicity assay. ^{51}Cr-labeled target cells were divided into aliquots in 96-well plates (10^4 cells/well). Effector PBMC cells (5×10^5 cells/well) were then added to each well in the presence or absence of rituximab (0 to 31.25 μg/mL) and incubated for 4 hours at 37°C. Supernatants were obtained after a brief centrifugation and measured on a γ-ray counter (PerkinElmer). ^{51}Cr-labeled target cells without antibodies were lysed completely by NP-40 (2% final concentration) and used as a positive control (the maximal ^{51}Cr release). The percentage of lysed cells was calculated using the following formula: % cell lysis = [(experimental release (cpm) − background (cpm)/(maximal release (cpm) − background (cpm))] × 100%, where cpm indicates counts per minute.

Results

CD20-negative phenotypic change after treatment with rituximab

A total of 124 patients with CD20-positive B-cell malignancies were treated with rituximab-combined chemotherapy from September 2001 to December 2006 (Table 1). All patients were diagnosed with CD20-positive B-cell lymphomas by IHC and/or FCM analyses using their tumor tissue specimens. Thirty-six patients (29.0%) showed relapse and progression (response; relapse/progression of disease [RD/PD] in Table 1) of their disease after or during chemotherapies with rituximab. Tumor cells from 19 of these 36 patients (52.8%) were resampled at the time of RD/PD, and CD20 protein expression was analyzed by IHC and/or FCM. CD20 protein expression was not detected or was significantly decreased in 5 patients (DLBCL, 3 patients; FL, 2 patients). Therefore, in 26.3% of patients whose tumor cells were resampled at the time of RD/PD, a CD20-negative phenotypic transformation after rituximab treatment was observed.

Clinical and laboratory features of patients with a CD20-negative phenotypic change

The clinical features of the 5 patients with a CD20-negative phenotypic change after rituximab treatment are shown in Table 2. Initially, 3 patients were diagnosed with DLBCL and 2 patients were diagnosed with FL. They were treated with chemotherapy with rituximab (375 mg/m^2) repeatedly until a CD20-negative phenotypic change was observed. Four to 14 cycles of rituximab were administered. These 5 patients showed relapse or progression from 2 to 81 months after their first treatment with rituximab. Histologic transformation from FL was observed in 2 patients, resulting in all 5 patients being diagnosed histologically as DLBCL at the time of RD/PD. Tumor cell infiltration into the bone marrow was observed in all 5 patients. A CD20 protein-negative phenotype was confirmed by IHC (Figure 1) and FCM in all 5 cases. In 3 patients, mRNA from tumor tissues was available, and CD20 mRNA expression was faintly observed using RT-PCR. Although all 5 patients received salvage chemotherapy without rituximab, they all died from disease progression within 11 months of the confirmation of CD20-negative transformation. The clinical outcomes of these patients who showed RD/PD after treatment with rituximab-containing chemotherapy are shown in Table 3. The 5 patients with CD20-negative RD/PD tended to have a shorter survival time than with CD20-positive RD/PD (100% vs 35.7% died). However, statistical significance could not be determined because of the variable disease status of each patient, including different backgrounds, salvage chemotherapies, and other factors. More patients must be studied to further analyze this apparent trend.

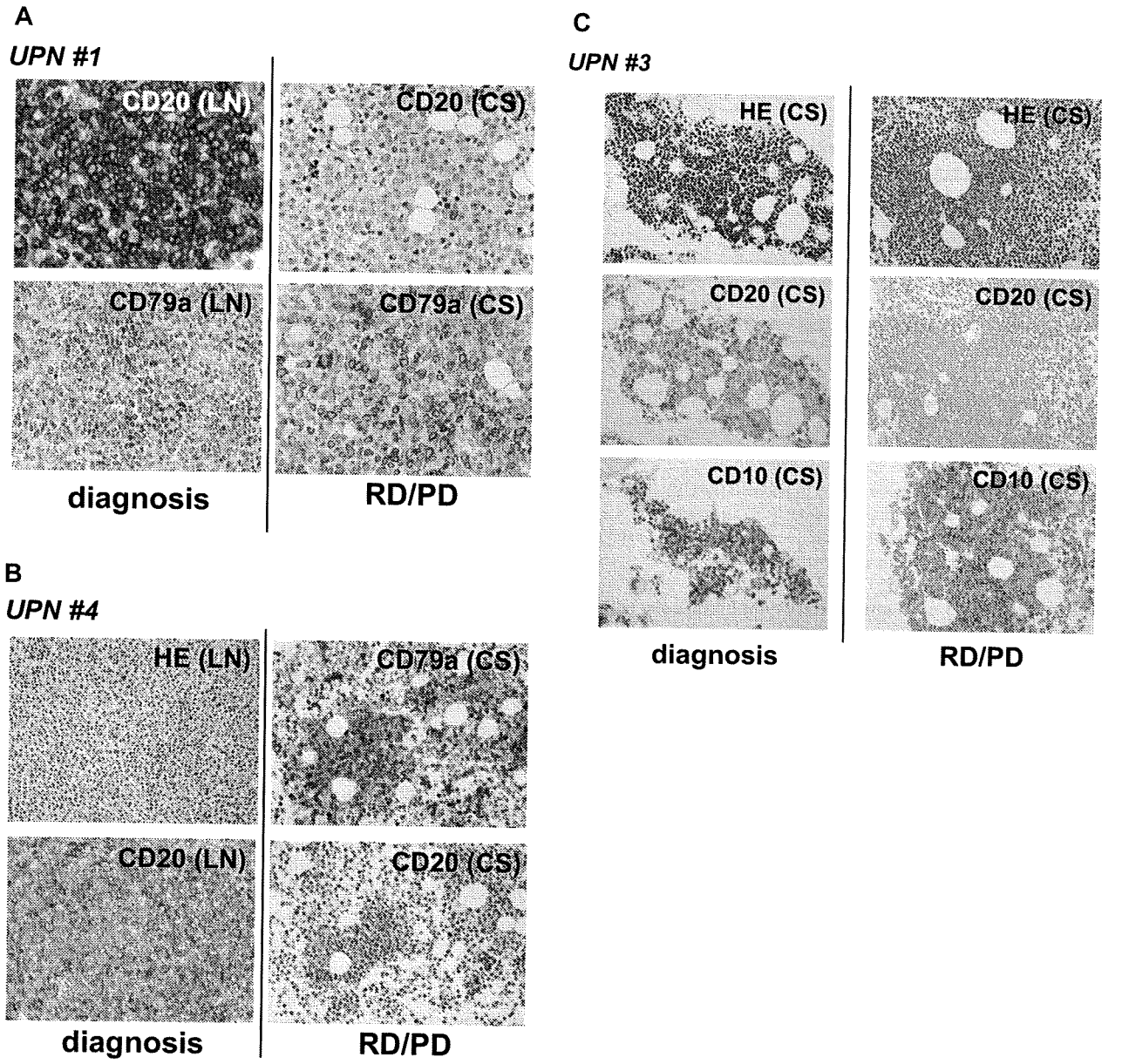

Figure 1. CD20 protein–negative phenotypic changes in CD20-positive B-cell lymphoma patients after treatment with rituximab-containing chemotherapy. Tissue samples (LN, lymph nodes; CS, bone marrow clot section) obtained from UPNs 1 (A), 4 (B), and 3 (C) in Table 2 were analyzed by IHC using anti-CD20, anti-CD79a, and anti-CD10 antibodies. Anti-CD79a antibody was used for detection of B cells. Note that CD20 was positive at the time of initial diagnosis in these patients, and that the CD20-negative phenotypic change was observed during the relapse/progression period. Original magnifications, ×400 (A) and ×200 (B,C) (Olympus BX51TF microscope, Olympus, Tokyo, Japan, and Nikon DS-Fi1 camera, Nikon, Tokyo, Japan). HE indicates hematoxylin and eosin staining; and RD/PD, relapse/progression of disease.

Table 3. Response against salvage chemotherapies for the 36 patients who showed relapse or PD after rituximab-containing chemotherapies.

	CD20 expression		
Response	−	+	N.D.
CR	0	5	3
PR	0	1	3
SD	0	1	1
RD/PD	0	2	2
Death	5	5	8
Total cases	5	14	17

These outcomes were evaluated in July, 2007.

CR indicates complete remisson; PR, partial response; SD, stable disease; RD/PD, relapse/progression; and N.D., Not determined.

Genetic abnormalities in the *CD20* gene

Genomic DNA mutations in the coding sequence (CDS) of the *CD20* gene, also known as the *MS4A1* gene, were also analyzed in the 5 patients. If the mutations were located in specific domains that are recognized by anti-CD20 antibodies including rituximab, those mutations might be related to resistance to rituximab and/or the CD20-negative phenotype. As indicated in Table 2, the change in serine 97 to phenylalanine (S97F; TCC → TTC) in unique patient number (UPN) 1 and valine 247 to isoleucine (V247I; GTT → ATT) in UPN 2 were confirmed in 2 clones each of 16 and 10 clones, respectively. In the other 3 cases, no genetic mutations in the *MS4A1* CDS were detected. Chromosomal analysis by G-banding was also performed using tumor cells obtained from each patient in both the initial diagnosis (CD20-positive) and at the time of RD/PD

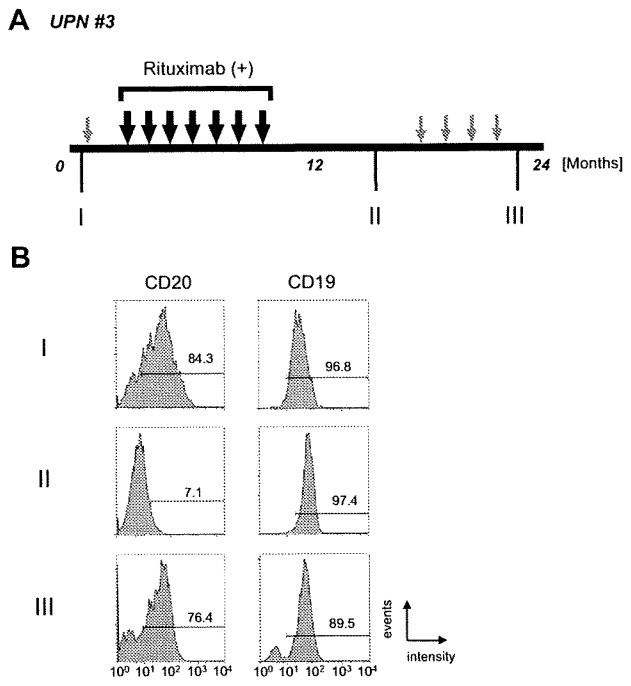

Figure 2. Alteration of CD20 protein expression on B-cell lymphoma cells during disease progression. (A) The clinical course of UPN 3 is depicted briefly. Large black arrows and smaller gray arrows indicate one course of combination chemotherapy with or without rituximab, respectively. Rituximab (375 mg/m^2 each) was administered 7 times. During the patient's 24-month clinical course, tumor cells were harvested at stages I, II, and III from lymph nodes, bone marrow, peripheral blood, and/or cerebral fluid. (B) FCM analysis using anti-CD20 and anti-CD19 antibodies was carried out using tumor cells from peripheral blood. Positive cells are shown in the black lines, and the percentage of positive cells is shown. Note that CD20 expression was observed at the initial diagnosis (I, 84.3%), and that the expression then diminished after treatment with chemotherapy with rituximab (II, 7.1%). Interestingly, CD20 protein expression was observed again at the terminal stage after several chemotherapy treatments without rituximab (III, 76.4%). On the other hand, CD19 expression level was stable throughout the clinical course.

(CD20-negative; Table S1, available on the *Blood* website; see the Supplemental Materials link at the top of the online article). Chromosomal abnormalities involving 11q12 containing the *MS4A1* gene were not observed.

Alteration of CD20 protein and mRNA expression levels after treatment with rituximab

As shown in Figure 1, CD20 protein expression by IHC analysis is altered after chemotherapy with rituximab. The clinical course of UPN 3 is depicted briefly in Figure 2A. FCM analyses using appropriate lymphoma tissues from lymph nodes, peripheral blood, bone marrow, and/or cerebral fluid were performed at admission (I), upon relapse after treatment with rituximab-containing combination chemotherapy (II), and at the end stage of disease after salvage chemotherapy without rituximab (III). The results of FCM analysis using peripheral blood, which contains lymphoma cells, are shown in Figure 2B. Interestingly, CD20 protein expression recognized by FCM analysis was significantly diminished at stage II, but was reversed at stage III. At stage II, CD20-negative lymphoma cell infiltration into the cerebral fluid was also confirmed by FCM analysis (data not shown). On the other hand, CD19 expression, which is also present on B-cell lymphoma cells, was detected constantly throughout the clinical course (Figure 2B right column). Semiquantitative RT-PCR (Figure 3A) and quantitative RT-PCR (Figure 3B) show that the mRNA expression level of *CD20* was significantly altered in each stage. CD20 mRNA expression was faintly observed at stage II (Figure 3B column 4) when CD20 protein expression was barely detectable with FCM (Figure 2B) and IHC (Figure 1C). In UPN 4, CD20 mRNA expression levels were determined by RT-PCR using tumor samples obtained before and after treatment with rituximab-containing chemotherapy (Figure 3C,D). Similar to UPN 3, CD20 mRNA expression was significantly decreased, and no protein expression was detected with IHC (Figure 1B). These findings suggest that CD20 protein expression is mainly regulated at the transcriptional level, and that the expression may be down-regulated in patients who show CD20-negative transformation after treatment with rituximab.

Epigenetic regulation of *CD20* gene expression after treatment with rituximab

These findings suggest that CD20 expression is partly epigenetically regulated by factors such as rituximab treatment surrounding tumor cells, or that CD20-negative tumor cells are able to grow selectively during rituximab treatment. If the CD20-negative B cells still possess the capability to express CD20 protein, we hypothesized that some epigenetic drugs[38,39] may be able to stimulate the *CD20* transcription. First, we examined *CD20* transcription after treatment with 5-Aza using primary tumor cells derived from cerebral fluid of UPN 3 at stage II in Figure 2A, which

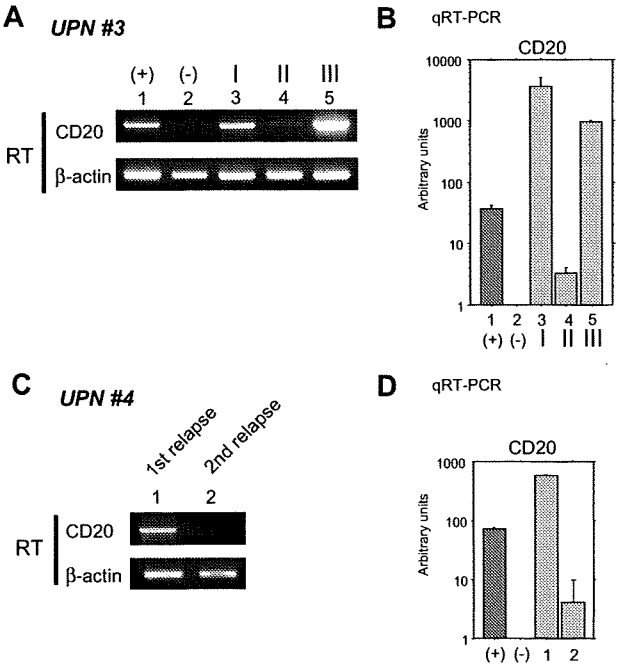

Figure 3. Alteration of CD20 mRNA expression in B-cell lymphoma cells during the clinical course. (A) RT-PCR (RT) was performed using total RNA from the same tumor cells as in Figure 2B (UPN 3 in Table 2). As positive and negative controls, total RNA from Raji and 293T cells was used (lanes 1 and 2), respectively. I, II, and III (lanes 3-5) correspond to the clinical stages depicted in Figure 2A. (B) Quantitative RT-PCR was performed using the same RNA as in panel A. Arbitrary units of CD20 mRNA expression are indicated in the vertical axis. Note that faint expression of CD20 mRNA could be seen at stage II (column 4) despite a loss of CD20 surface protein expression as shown in Figure 2B. (C) CD20 mRNA expression in the lymphoma cells of UPN 4 (Table 2) was also analyzed. Tumor cells were derived from cerebral fluid at the first relapse after chemotherapy without rituximab (lane 1). Although complete remission was obtained after using rituximab-containing salvage chemotherapy, a second relapse occurred. Tumor cells were once again harvested from this patient's cerebral fluid and analyzed (lane 2). (D) Quantitative RT-PCR was also performed using the same RNA as in (C). Note that CD20 mRNA expression was significantly diminished but could still be observed. In these cells, CD20 protein expression was undetectable using FCM or IHC as indicated in Table 2. Positive and negative controls derived from Raji and 293T cells are indicated by + and −, respectively.

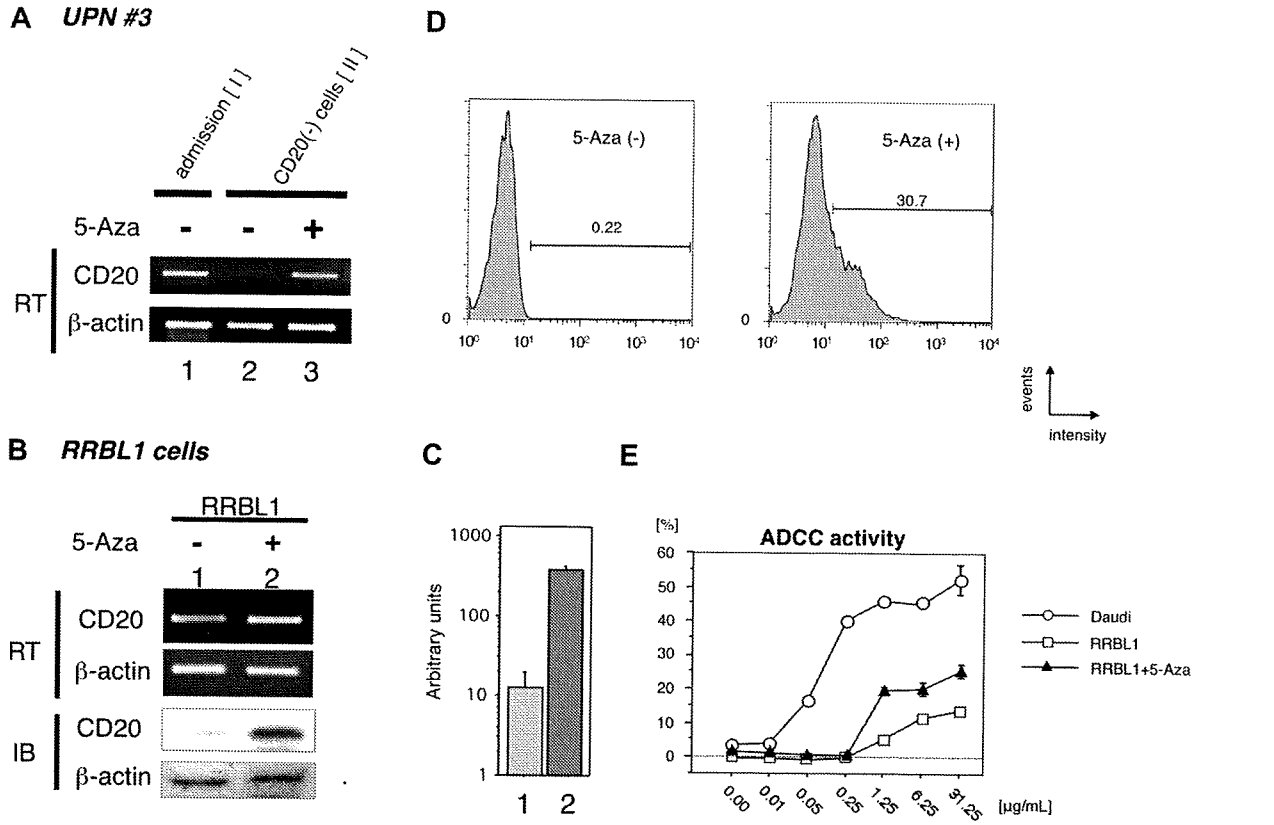

Figure 4. Restoration of CD20 mRNA and protein expression by treatment with the DNA methyltransferase inhibitor 5-Aza. (A) Primary B-cell lymphoma cells, which showed a CD20 protein-negative phenotype from UPN 3, were incubated with or without 5-Aza. Total RNA was prepared, and semiquantitative RT-PCR was performed. Restoration of CD20 mRNA expression after treatment with 5-Aza was observed in lane 3. As a positive control, tumor cells obtained at the initial diagnosis of that same patient were used in lane 1. (B) The CD20 protein-negative B-cell lymphoma cell line RRBL1,[32] which was derived from UPN 5 in Table 2, was incubated in culture medium with or without 5-Aza. After preparation of total RNA and whole-cell lysates from these cells, semiquantitative RT-PCR and immunoblotting (IB) were performed. Up-regulation of CD20 mRNA and protein expression was observed as shown in lane 2. (C) Quantitative RT-PCR was performed using the same mRNA as in (B). We observed an up-regulation of more than 10-fold in CD20 mRNA after treatment with 5-Aza (column 2). (D) RRBL1 cells were treated with 5-Aza under the same conditions as in (B), and FCM analysis using anti-CD20 antibody was performed. After treatment with 5-Aza, 30.7% of RRBL1 cells showed a CD20-positive phenotype. Positive cells are shown with black lines, and the percentage of positive cells is also shown. (E) In vitro ADCC analysis using the ^{51}Cr-release assay. Cells from the CD20-positive B-cell lymphoma/leukemia cell lines Daudi and RRBL1 treated with or without 5-Aza were used for this assay. In Daudi cells (○), but not in RRBL1 cells (□), cytotoxic activity was observed in the presence of rituximab in a dose-dependent manner. Partial restoration of rituximab sensitivity in RRBL1 cells was observed after treatment with 5-Aza (▲). Error bars indicate plus or minus 1 standard deviation.

showed a CD20-negative phenotype. As a CD20-positive control, lymphoma cells at the initial diagnosis from the same patient were used (Figure 4A lane 1). After treatment with 5-Aza in vitro, significant stimulation of CD20 expression was observed (Figure 4 lane 3).

Previously, we established the CD20-negative B-cell lymphoma cell line RRBL1,[32] which was derived from CD20-negative tumor cells in peripheral blood from a patient (UPN 5 in Table 2). Next, we performed the same assay using these cells (Figure 4B), and we were able to show up-regulation of CD20 mRNA expression (Figure 4B,C). CD20 protein expression induction was also confirmed by immunoblotting (Figures 4B, IB). Thus, these data, showing that CD20 expression could be stimulated within a few days, suggested that CD20 expression is down-regulated by epigenetic mechanisms.

Restoration of rituximab sensitivity in CD20-negative cells after treatment with 5-Aza in vitro

From these findings, we hypothesized that rituximab sensitivity would be restored if we could stimulate CD20 protein expression on the surface of CD20-negative transformed lymphoma cells. To test this hypothesis, we performed FCM analysis and an in vitro ADCC assay using RRBL1 cells with or without 5-Aza treatment. As shown in Figure 4D, CD20 protein expression was induced on the surface of 30.7% of RRBL1 cells after treatment with 5-Aza. Using these cells with or without 5-Aza treatment, an in vitro ^{51}Cr-release assay was performed to confirm ADCC activity induced by rituximab (Figure 4E). Daudi cells were used as CD20-positive rituximab-sensitive control cells. In the presence of rituximab, cell death was observed in a dose-dependent manner in Daudi cells. In contrast, the percentage of RRBL1 cells undergoing cell death was significantly lower despite the high concentration of rituximab. RRBL1 cells treated with 5-Aza showed partial rituximab sensitivity compared with RRBL1 cells not treated with 5-Aza. These experiments were done in triplicate and repeated at least 3 times, with similar results. These data suggest that CD20 expression and rituximab sensitivity could be restored in some cases using epigenetic drug treatment even when CD20-negative transformation results from rituximab treatment. Further experiments using patients' primary samples and an in vivo system will be required to further explore this idea.

Discussion

Rituximab is a clinically important antitumor monoclonal antibody targeting the CD20 surface antigen expressed on B-cell malignancies. However, its effectiveness is sometimes unsatisfactory since a significant percentage of patients treated with rituximab-containing

chemotherapy showed relapse or progression.[3,6,40] In this report, we also estimated that RD/PD after treatment with rituximab was observed in almost 30% of B-cell lymphoma patients after treatment with combination chemotherapies with rituximab. Importantly, not all patients who show RD/PD demonstrate resistance to rituximab. In fact, some patients were sensitive to retreatment with rituximab-containing salvage chemotherapies (data not shown). We may need to define "rituximab resistance" more carefully by monitoring each patient's clinical course.

A CD20-negative phenotypic change was observed in 26.3% of patients for whom tumor resampling (rebiopsy) was carried out (Table 1). We generally perform rebiopsies when tumor progression becomes very aggressive or when the manner of tumor expansion significantly changes during clinical observation. If we had carried out resampling on every RD/PD patient, the percentage of patients with CD20-negative transformations may have been much lower. Thus, examination of more patients will be critical. One important observation about the CD20-negative phenotypic change is that all 5 patients died from their disease progression within 1 year after showing a CD20-negative transformation (Tables 2,3). This observation may indicate that a loss of CD20 expression is partly related to poor prognosis. In our study, however, patients' backgrounds varied (eg, age, sex, pathologic findings, chemotherapy regimens, and organ function). A larger patient sample is warranted to determine the significance of the loss of CD20 expression.

It is noteworthy that CD20 mRNA expression was confirmed by RT-PCR even in those tumor cells that showed a CD20 protein-negative phenotype using IHC, FCM, and immunoblotting (Figure 3). In one case (Figure 3, UPN 3), expression of CD20 mRNA and protein were observed again after salvage chemotherapy without rituximab. Clonal evolution may be one reason for the alteration of CD20 mRNA and protein expression patterns in the same patient either with or without rituximab. However, our finding of the restoration of CD20 mRNA and protein expression within 3 days after treatment with 5-Aza (Figure 4) may instead support the idea that expression is regulated by epigenetic mechanisms, rather than by the alteration of several tumor clones.

We cannot exclude the possibility that genetic alteration in tumor cells that affects the expression of transcription factors PU.1, Pip, and Oct2, which are thought to be critical for *MS4A1* (*CD20*) gene expression,[41] may contribute to the aberrant *CD20* transcriptional regulation. We analyzed the methylation status of cytosine guanine dinucleotides (CpGs) in *CD20* promoters almost 1000 bp upstream from the transcription start site to determine the mechanism of transcription up-regulation by 5-Aza treatment. Interestingly, CpG islands do not exist in the promoter site, and only 4 CG sequences can be observed in that region. Methylation of the 4 CG sites was not observed in the tumor cells from UPN 5 and RRBL1 cells using bisulfite sequencing (data not shown). Mechanisms other than DNA methylation of the *CD20* promoter may also be responsible for aberrant transcription down-regulation.

It is also possible that down-regulation of CD20 protein via such mechanisms as microRNA, protein folding, exportation, or glycosylation may occur. A recent report suggested the possibility that both *CD20* gene expression (at the pre- and posttranscriptional level) and protein down-regulation are related to the loss of CD20 protein expression after treatment with rituximab in vitro, resulting in rituximab resistance.[10] In addition, down-regulation of CD20 protein surface expression by internalization into the cytoplasm was also observed in some specific cases.[16,42] Further molecular analysis of the down-regulation of CD20 protein after treatment with rituximab is needed.

Another interesting finding in our study is that all of the patients showed a CD20-negative phenotypic change were diagnosed as DLBCL. Two cases were diagnosed as FL at their first admission, but both were transformed into DLBCL when a CD20-negative change was observed. Furthermore, a CD20-negative change was confirmed in all 5 cases using tumor cells derived from the bone marrow and/or cerebral fluid. These findings may suggest that the clinical entity and progression pattern is partly related to CD20-negative phenotypic transformation. Further studies will be needed to confirm this idea.

Genetic mutations in the *CD20* coding sequence were also observed in 2 cases, as shown in Table 2. These mutations led to amino acid alterations, including S97F and V247I, which are located at the second transmembrane domain and the C-terminal intracellular domain, respectively. A recent report suggested that neither site is recognized directly by rituximab.[43] Although it is possible that these alterations led to a conformational change in the CD20 protein that interferes with rituximab binding, a more attractive explanation may be that the loss of expression is much more critical for resistance to rituximab than we originally suspected. Preliminary data using fluorescence-labeled rituximab indicate that rituximab fails to bind to RRBL1 cells (CD20-negative B cells) in vitro (data not shown), and that ADCC and complement-dependent cytotoxicity (CDC) activity in vitro are significantly lower than in CD20-positive B cells (CDC; data not shown). These data suggest that the loss of antibody binding due to the down-regulation of antigen expression is one critical mechanism underlying rituximab resistance. Further investigation will be needed to expand these observations.

Our observations also revealed a population of cells that are rituximab-resistant despite the presence of CD20 protein expression as observed by FCM, IHC, and immunoblotting (data not shown). In those patients, molecular mechanisms other than a loss of protein expression may have occurred, such as an amino acid alteration resulting from a genetic mutation of the *MS4A1* gene, a posttranslational modification of the CD20 protein, abnormalities in the CD20 signal transduction pathway, antiapoptotic mechanisms of tumor cells, or aberrant metabolism of rituximab.[9,44,45] The detailed mechanisms of these and other possibilities are still unclear.

Finally, in the specific cases reported herein, 5-Aza can stimulate CD20 mRNA and protein expression, resulting in the restoration of rituximab sensitivity in vitro. The DNA methyltransferase inhibitors 5-azacytidine and 5-Aza have been used in patients suffering from hematologic malignancies such as myelodysplastic syndrome.[38,39,46] In the future, a combination of molecular targeting therapy using 5-Aza and rituximab may prove to be a unique strategy as a salvage therapy for CD20-negative transformed B-cell malignancies in certain patients. Further analysis of patients' primary cells and in vivo analysis using mouse xenograft lymphoma models are required.

Acknowledgments

We thank Tomoka Wakamatsu, Yukie Konishi, Mari Otsuka, Eriko Ushida, and Chieko Kataoka for valuable laboratory assistance. We also thank Yoko Kajiura, Yasuhiko Miyata, and Yuka Nomura for the FCM data analysis.

This work was supported in part by a Grant-in-Aid for Cancer Research (19-8) from the Ministry of Health, Labor and Welfare, a Grant-in-Aid from the National Institute of Biomedical Innovation, and

a Grant-in-Aid for Scientific Research (20591116) from the Ministry of Education, Culture, Sports, Science and Technology, Japan.

Authorship

J.H. and A.T. designed experiments, performed research, analyzed data, and wrote the paper; T.S. and K.S. prepared clinical samples and performed research; M.I. and S.N. performed pathologic analyses; H.K. and T.K. analyzed data, designed experiments, and interpreted data; and T.N. supervised experiments and wrote the paper.

Conflict-of-interest disclosure: H.K. is a consultant for a Kyowa Hakko Kogyo (Tokyo, Japan), and T.K. is funded by Chugai Pharmaceutical (Tokyo, Japan) and for Zenyaku Kogyo (Tokyo, Japan). The other authors declare no competing financial interests.

Correspondence: Akihiro Tomita, Department of Hematology and Oncology, Nagoya University Graduate School of Medicine, Tsurumai-cho 65, Showa-ku, Nagoya 466-8550, Japan; e-mail; atomita@med.nagoya-u.ac.jp.

References

1. Cheson BD. Monoclonal antibody therapy for B-cell malignancies. Semin Oncol. 2006;33:S2-14.
2. Imai K, Takaoka A. Comparing antibody and small-molecule therapies for cancer. Nat Rev Cancer. 2006;6:714-727.
3. Coiffier B, Lepage E, Briere J, et al. CHOP chemotherapy plus rituximab compared with CHOP alone in elderly patients with diffuse large-B-cell lymphoma. N Engl J Med. 2002;346:235-242.
4. Herold M, Haas A, Srock S, et al. Rituximab added to first-line mitoxantrone, chlorambucil, and prednisolone chemotherapy followed by interferon maintenance prolongs survival in patients with advanced follicular lymphoma: an East German Study Group Hematology and Oncology Study. J Clin Oncol. 2007;25:1986-1992.
5. Forstpointner R, Unterhalt M, Dreyling M, et al. Maintenance therapy with rituximab leads to a significant prolongation of response duration after salvage therapy with a combination of rituximab, fludarabine, cyclophosphamide, and mitoxantrone (R-FCM) in patients with recurring and refractory follicular and mantle cell lymphomas: results of a prospective randomized study of the German Low Grade Lymphoma Study Group (GLSG). Blood. 2006;108:4003-4008.
6. Habermann TM, Weller EA, Morrison VA, et al. Rituximab-CHOP versus CHOP alone or with maintenance rituximab in older patients with diffuse large B-cell lymphoma. J Clin Oncol. 2006;24:3121-3127.
7. Pfreundschuh M, Trumper L, Osterborg A, et al. CHOP-like chemotherapy plus rituximab versus CHOP-like chemotherapy alone in young patients with good-prognosis diffuse large-B-cell lymphoma: a randomised controlled trial by the MabThera International Trial (MInT) Group. Lancet Oncol. 2006;7:379-391.
8. Igarashi T, Kobayashi Y, Ogura M, et al. Factors affecting toxicity, response and progression-free survival in relapsed patients with indolent B-cell lymphoma and mantle cell lymphoma treated with rituximab: a Japanese phase II study. Ann Oncol. 2002;13:928-943.
9. Smith MR. Rituximab (monoclonal anti-CD20 antibody): mechanisms of action and resistance. Oncogene. 2003;22:7359-7368.
10. Czuczman MS, Olejniczak S, Gowda A, et al. Acquirement of rituximab resistance in lymphoma cell lines is associated with both global CD20 gene and protein down-regulation regulated at the pretranscriptional and posttranscriptional levels. Clin Cancer Res. 2008;14:1561-1570.
11. Olejniczak SH, Hernandez-Ilizaliturri FJ, Clements JL, Czuczman MS. Acquired resistance to rituximab is associated with chemotherapy resistance resulting from decreased Bax and Bak expression. Clin Cancer Res. 2008;14:1550-1560.
12. Macor P, Tripodo C, Zorzet S, et al. In vivo targeting of human neutralizing antibodies against CD55 and CD59 to lymphoma cells increases the antitumor activity of rituximab. Cancer Res. 2007; 67:10556-10563.
13. Cruz RI, Hernandez-Ilizaliturri FJ, Olejniczak S, et al. CD52 over-expression affects rituximab-associated complement-mediated cytotoxicity but not antibody-dependent cellular cytotoxicity: preclinical evidence that targeting CD52 with alemtuzumab may reverse acquired resistance to rituximab in non-Hodgkin lymphoma. Leuk Lymphoma. 2007;48:2424-2436.
14. Terui Y, Sakurai T, Mishima Y, et al. Blockade of bulky lymphoma-associated CD55 expression by RNA interference overcomes resistance to complement-dependent cytotoxicity with rituximab. Cancer Sci. 2006;97:72-79.
15. Takei K, Yamazaki T, Sawada U, Ishizuka H, Aizawa S. Analysis of changes in CD20, CD55, and CD59 expression on established rituximab-resistant B-lymphoma cell lines. Leuk Res. 2006; 30:625-631.
16. Jilani I, O'Brien S, Manshuri T, et al. Transient down-modulation of CD20 by rituximab in patients with chronic lymphocytic leukemia. Blood. 2003;102:3514-3520.
17. Bannerji R, Kitada S, Flinn IW, et al. Apoptotic-regulatory and complement-protecting protein expression in chronic lymphocytic leukemia: relationship to in vivo rituximab resistance. J Clin Oncol. 2003;21:1466-1471.
18. Treon SP, Mitsiades C, Mitsiades N, et al. Tumor cell expression of CD59 is associated with resistance to CD20 serotherapy in patients with B-cell malignancies. J Immunother. 2001;24:263-271.
19. Golay J, Lazzari M, Facchinetti V, et al. CD20 levels determine the in vitro susceptibility to rituximab and complement of B-cell chronic lymphocytic leukemia: further regulation by CD55 and CD59. Blood. 2001;98:3383-3389.
20. Kinoshita T, Nagai H, Murate T, Saito H. CD20-negative relapse in B-cell lymphoma after treatment with rituximab. J Clin Oncol. 1998;16:3916.
21. Schmitz K, Brugger W, Weiss B, Kaiserling E, Kanz L. Clonal selection of CD20-negative non-Hodgkin's lymphoma cells after treatment with anti-CD20 antibody rituximab. Br J Haematol. 1999;106:571-572.
22. Davis TA, Czerwinski DK, Levy R. Therapy of B-cell lymphoma with anti-CD20 antibodies can result in the loss of CD20 antigen expression. Clin Cancer Res. 1999;5:611-615.
23. Chu PG, Chen YY, Molina A, Arber DA, Weiss LM. Recurrent B-cell neoplasms after rituximab therapy: an immunophenotypic and genotypic study. Leuk Lymphoma. 2002;43:2335-2341.
24. Massengale WT, McBurney E, Gurtler J. CD20-negative relapse of cutaneous B-cell lymphoma after anti-CD20 monoclonal antibody therapy. J Am Acad Dermatol. 2002;46:441-443.
25. Kennedy GA, Tey SK, Cobcroft R, et al. Incidence and nature of CD20-negative relapses following rituximab therapy in aggressive B-cell non-Hodgkin's lymphoma: a retrospective review. Br J Haematol. 2002;119:412-416.
26. Alvaro-Naranjo T, Jaen-Martinez J, Guma-Padro J, Bosch-Princep R, Salvado-Usach MT. CD20-negative DLBCL transformation after rituximab treatment in follicular lymphoma: a new case report and review of the literature. Ann Hematol. 2003;82:585-588.
27. Clarke LE, Bayerl MG, Ehmann WC, Helm KF. Cutaneous B-cell lymphoma with loss of CD20 immunoreactivity after rituximab therapy. J Cutan Pathol. 2003;30:459-462.
28. Haidar JH, Shamseddine A, Salem Z, et al. Loss of CD20 expression in relapsed lymphomas after rituximab therapy. Eur J Haematol. 2003;70:330-332.
29. Rawal YB, Nuovo GJ, Frambach GE, Porcu P, Baiocchi RA, Magro CM. The absence of CD20 messenger RNA in recurrent cutaneous B-cell lymphoma following rituximab therapy. J Cutan Pathol. 2005;32:616-621.
30. Goteri G, Olivieri A, Ranaldi R, et al. Bone marrow histopathological and molecular changes of small B-cell lymphomas after rituximab therapy: comparison with clinical response and patients outcome. Int J Immunopathol Pharmacol. 2006; 19:421-431.
31. Ferreri AJ, Dognini GP, Verona C, Patriarca C, Doglioni C, Ponzoni M. Re-occurrence of the CD20 molecule expression subsequent to CD20-negative relapse in diffuse large B-cell lymphoma. Haematologica. 2007;92:e1-2.
32. Tomita A, Hiraga J, Kiyoi H, et al. Epigenetic regulation of CD20 protein expression in a novel B-cell lymphoma cell line, RRBL1, established from a patient treated repeatedly with rituximab-containing chemotherapy. Int J Hematol. 2007;86: 49-57.
33. Harris NL, Jaffe ES, Diebold J, et al. World Health Organization classification of neoplastic diseases of the hematopoietic and lymphoid tissues: report of the Clinical Advisory Committee meeting-Airlie House, Virginia, November 1997. J Clin Oncol. 1999;17:3835-3849.
34. Cheson BD, Horning SJ, Coiffier B, et al. Report of an international workshop to standardize response criteria for non-Hodgkin's lymphomas: NCI Sponsored International Working Group. J Clin Oncol. 1999;17:1244.
35. Ninomiya M, Abe A, Yokozawa T, et al. Establishment of a myeloid leukemia cell line, TRL-01, with MLL-ENL fusion gene. Cancer Genet Cytogenet. 2006;169:1-11.
36. Atsumi A, Tomita A, Kiyoi H, Naoe T. Histone deacetylase 3 (HDAC3) is recruited to target promoters by PML-RARalpha as a component of the N-CoR co-repressor complex to repress transcription in vivo. Biochem Biophys Res Commun. 2006;345:1471-1480.
37. Tomita A, Buchholz DR, Obata K, Shi YB. Fusion protein of retinoic acid receptor alpha with promyelocytic leukemia protein or promyelocytic leukemia zinc finger protein recruits N-CoR-TBLR1 corepressor complex to repress transcription in vivo. J Biol Chem. 2003;278: 30788-30795.
38. Egger G, Liang G, Aparicio A, Jones PA. Epigenetics in human disease and prospects for epigenetic therapy. Nature. 2004;429:457-463.
39. Yoo CB, Jones PA. Epigenetic therapy of cancer: past, present and future. Nat Rev Drug Discov. 2006;5:37-50.

40. van Oers MH, Klasa R, Marcus RE, et al. Rituximab maintenance improves clinical outcome of relapsed/resistant follicular non-Hodgkin's lymphoma, both in patients with and without rituximab during induction: results of a prospective randomized phase III intergroup trial. Blood. 2006;108;3295-3301.

41. Himmelmann A, Riva A, Wilson GL, Lucas BP, Thevenin C, Kehrl JH. PU.1/Pip and basic helix loop helix zipper transcription factors interact with binding sites in the CD20 promoter to help confer lineage- and stage-specific expression of CD20 in B lymphocytes. Blood. 1997;90: 3984-3995.

42. Lapalombella R, Yu B, Triantafillou G, et al. Lenalidomide down-regulates the CD20 antigen and antagonizes direct and antibody-dependent cellular cytotoxicity of rituximab on primary chronic lymphocytic leukemia cells. Blood. 2008;113: 5180-5185.

43. Binder M, Otto F, Mertelsmann R, Veelken H, Trepel M. The epitope recognized by rituximab. Blood. 2006;108:1975-1978.

44. Bonavida B. Rituximab-induced inhibition of antiapoptotic cell survival pathways: implications in chemo/immunoresistance, rituximab unresponsiveness, prognostic and novel therapeutic interventions. Oncogene. 2007;26:3629-3636.

45. Glennie MJ, French RR, Cragg MS, Taylor RP. Mechanisms of killing by anti-CD20 monoclonal antibodies. Mol Immunol. 2007;44:3823-3837.

46. Laird PW. Cancer epigenetics. Hum Mol Genet. 2005;14:R65-R76.

doi:10.1111/j.1600-0609.2009.01324.x

LETTER TO THE EDITOR

Acute promyelocytic leukemia harboring a *STAT5B-RARA* fusion gene and a G596V missense mutation in the STAT5B SH2 domain of the *STAT5B-RARA*

To the Editor:

Introduction of all-*trans* retinoic acid (ATRA) has been the major breakthrough in the treatment of acute promyelocytic leukemia (APL) with a characteristic t(15;17) translocation (1, 2). With a great interest we read the report regarding the APL patient with STAT5B-RARα (3). To date, there are only three reported APL patients who harbor the STAT5B-RARα (3–6), therefore, clinical features of this particular subtype, response to therapy and its pathogenesis remain to be determined. This study describes the fourth APL patient harboring the STAT5B-RARα.

A 41-yr-old Japanese man was admitted to our hospital because of petechiae and fever in July 2006. His hemoglobin was 9.5 g/dL, platelet count was 51×10^9/L, and leukocyte count was 77.8×10^9/L with 91.2% abnormal promyelocytes (Fig. 1A). Promyelocytes were positive for CD13 and CD33 but negative for CD34 and

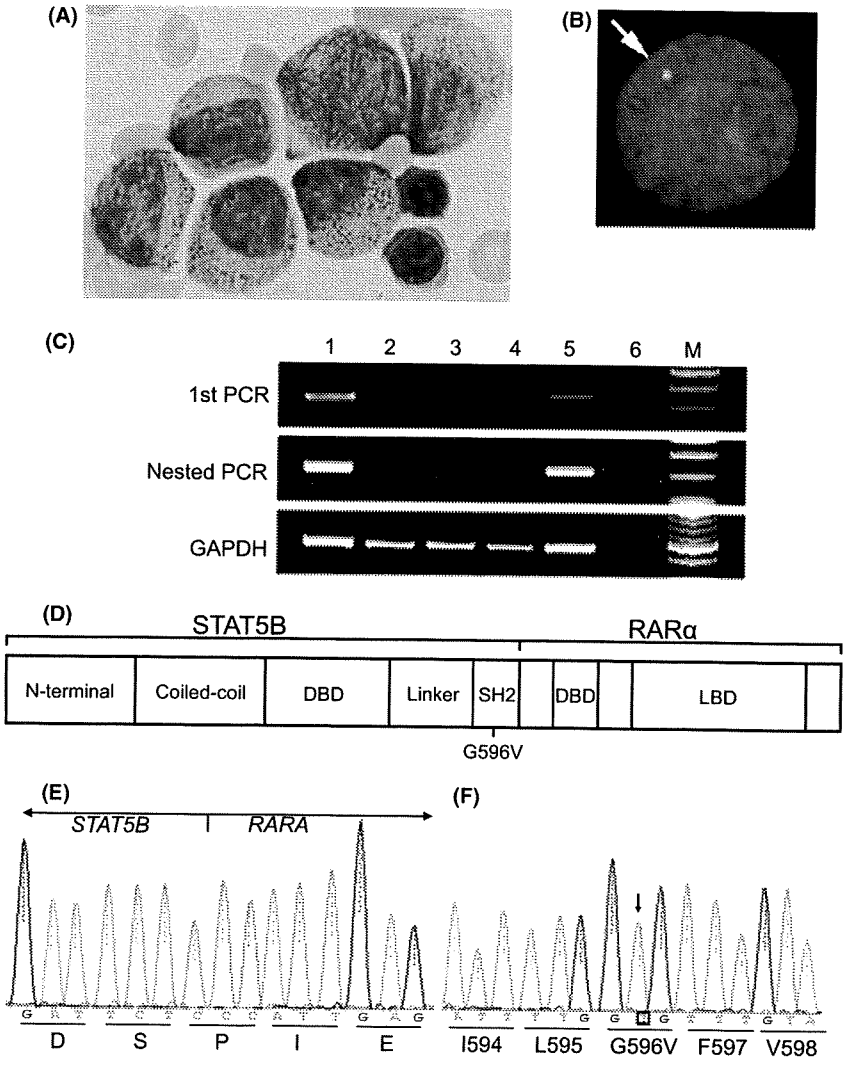

Figure 1 *STAT5B-RARA* fusion gene with G596V mutation in a patient with acute promyelocytic leukemia. (A) Promyelocytes had abundant azurophilic granules and faggot cells were also seen. Although the majority of promyelocytes were morphologically consistent with typical APL cells, there were some relatively mature cells with dense nuclei and hypergranulation. (B) Metaphase fluorescence *in situ* hybridization using *PML* and *RARA* dual fusion probes (Vysis, Abbott Molecular Inc. Des Plaines, IL, USA) showed one *RARA* (green) signal on chromosome 17 and two *PML* (red) signals on chromosome 15, but no yellow fusion signal in 98% of cells. (C) RT-PCR analysis of *STAT5B-RARA* fusion transcripts in bone marrow cells at diagnosis and relapse (lanes 1 and 5), after first complete remission (lanes 2 and 3) and after second complete remission (lane 4). Lane 6 shows no template. Lane M denotes DNA marker. (D) Schematic representation of STAT5B-RARα and G596V. (E, F) Chromatograph showing the breakpoint and the STAT5B G596V mutation in the fusion gene.

HLA-DR. Cytogenetic analysis of the bone marrow cells revealed 47,XY,del(9)(q?),add(17)(q12),+mar1[3]/48,XY, idem,+mar1[17]. Fibrin and fibrinogen degradation products were 344.0 μg/mL and activity of α2 plasmin inhibitor was 16%. A diagnosis of APL and disseminated intravascular coagulation (DIC) with fibrinolysis was made.

After one course of ATRA combined with cytarabine and idarubicin (2), the patient achieved a complete remission (CR) although ATRA-induced granulocytic differentiation was not observed. Moreover, he showed mild DIC during induction chemotherapy, despite high initial leukocyte counts. After two additional courses of consolidation chemotherapy, meningeal relapse occurred. A second CR was achieved after administration of high-dose cytarabine combined with intrathecal chemotherapy, followed by whole-brain irradiation. Six months after second CR, relapse occurred in the marrow and the patient died of APL 17 months after diagnosis.

Fluorescence *in situ* hybridization analysis of the marrow cells at diagnosis showed a hemizygous deletion of *RARA*, but no *PML-RARA* fusion signal (Fig. 1B). No *RARA* fusion transcript with *PML*, *PLZF*, *NPM1*, or *NuMA1* was detected by RT-PCR (7). On the other hand, *STAT5B-RARA* fusion transcript was found in marrow cells (Fig. 1C,D). Sequence analysis of the *STAT5B-RARA* corresponded to that of a previously reported case of *STAT5B-RARA*-positive APL (Fig. 1D,E) (4). Interestingly, there was an additional point mutation within the STAT5B SH2 domain of the *STAT5B-RARA* (G596V) (Fig. 1D,F). Although neither the *STAT5B-RARA* nor the G596V missense mutation was detected in marrow cells during CR, we observed both alterations at the time of relapse (Fig. 1C).

The STAT5B-RARα interacts with a corepressor complex containing histone deacetylase activity and blocks differentiation of hematopoietic cells, which is not released by treatment with ATRA (8, 9). The STAT5B-RARα chimeric protein was mainly delocalized from the cytoplasm to the nucleus, implicating that leukemogenesis of this APL might result from deregulation of the JAK-STAT5, in addition to RA-RARα, signaling pathways (4). All STAT proteins possess an SH2 domain that plays an important role in the activation of STAT proteins. Moreover, the substituted amino acid, G596, is highly conserved in the SH2-domain containing proteins from *drosophila* to *mammals*. Therefore, the G596V mutation in STAT5B-RARα is possibly associated with leukemogenesis.

Acknowledgements

This work was supported in part by Grants-in-Aid for Scientific Research from the Japanese Ministry of Education, Culture, Sport, Science and Technology, and by Grants-in-Aid for Cancer Research from the Japanese Ministry of Health, Labor and Welfare.

References

1. Grimwade D, Biondi A, Mozziconacci MJ, Hagemeijer A, Berger R, Neat M, Howe K, Dastugue N, Jansen J, Radford-Weiss I, Lo Coco F, Lessard M, Hernandez JM, Delabesse E, Head D, Liso V, Sainty D, Flandrin G, Solomon E, Birg F, Lafage-Pochitaloff M. Characterization of acute promyelocytic leukemia cases lacking the classic t(15;17): results of the European Working Party. Groupe Francais de Cytogenetique Hematologique, Groupe de Francais d'Hematologie Cellulaire, UK Cancer Cytogenetics Group and BIOMED 1 European Community-Concerted Action "Molecular Cytogenetic Diagnosis in Haematological Malignancies". *Blood* 2000;**96**:1297–308.
2. Asou N, Kishimoto Y, Kiyoi H, Okada M, Kawai Y, Tsuzuki M, Horikawa K, Matsuda M, Shinagawa K, Kobayashi T, Ohtake S, Nishimura M, Takahashi M, Yagasaki F, Takeshita A, Kimura Y, Iwanaga M, Naoe T, Ohno R, Japan Adult Leukemia Study Group. A randomized study with or without intensified maintenance chemotherapy in patients with acute promyelocytic leukemia who have become negative for PML-RARalpha transcript after consolidation therapy: the Japan Adult Leukemia Study Group (JALSG) APL97 study. *Blood* 2007;**110**:59–66.
3. Kusakabe M, Suzukawa K, Nanmoku T, Obara N, Okoshi Y, Mukai HY, Hasegawa Y, Kojima H, Kawakami Y, Ninomiya H, Nagasawa T. Detection of the STAT5B-RARA fusion transcript in acute promyelocytic leukemia with the normal chromosome 17 on G-banding. *Eur J Haematol* 2008;**80**:444–7.
4. Arnould C, Philippe C, Bourdon V, Gr goire MJ, Berger R, Jonveaux P. The signal transducer and activator of transcription STAT5b gene is a new partner of retinoic acid receptor alpha in acute promyelocytic-like leukaemia. *Hum Mol Genet* 1999;**8**:1741–9.
5. Jonveaux P, Le Coniat M, Derre J, Flexor MA, Daniel MT, Berger R. Chromosome microdissection in leukemia: a powerful tool for the analysis of complex chromosomal rearrangements. *Genes Chromosomes Cancer* 1996;**15**:26–33.
6. Gallagher R.E., Paietta E., Cooper B., Ehmann W.C., Tallman M.S. Identification of a second acute promyelocytic leukemia (APL) patient with the STAT5b-RARα fusion gene among PML-RARα-negative Eastern Cooperative Oncology Group (ECOG) APL protocol registrants. *Blood* 2004;**104**:821a.
7. Matsuno N, Nanri T, Kawakita T, Mitsuya H, Asou N. A novel FLT3 activation loop mutation N841K in acute myeloblastic leukemia. *Leukemia* 2005;**19**:480–1.
8. Dong S, Tweardy DJ. Interactions of STAT5b-RARalpha, a novel acute promyelocytic leukemia fusion protein, with

retinoic acid receptor and STAT3 signaling pathways. *Blood* 2002;**99**:2637–46.
9. Maurer AB, Wichmann C, Gross A, Kunkel H, Heinzel T, Ruthardt M, Groner B, Grez M. The Stat5-RARalpha fusion protein represses transcription and differentiation through interaction with a corepressor complex. *Blood* 2002;**99**:2647–52.

Eisaku Iwanaga, Miki Nakamura, Tomoko Nanri, Toshiro Kawakita, Kentaro Horikawa, Hiroaki Mitsuya, Norio Asou

Department of Hematology, Kumamoto University School of Medicine, Kumamoto, Japan

Correspondence Norio Asou, MD, Department of Hematology, Kumamoto University School of Medicine, 1-1-1 Honjo, Kumamoto 860-8556, Japan.
Tel: +81 96 373 5156; Fax: +81 96 363 5265; e-mail: ktcnasou@gpo.kumamoto-u.ac.jp

Expression profiling of a hemopoietic cell survival transcriptome implicates osteopontin as a functional prognostic factor in AML

Jason A. Powell,[1] Daniel Thomas,[1] Emma F. Barry,[1] Chung H. Kok,[2] Barbara J. McClure,[3] Anna Tsykin,[4] L. Bik To,[2] Anna Brown,[2] Ian D. Lewis,[2] Kirsten Herbert,[5] Gregory J. Goodall,[6,7] Terence P. Speed,[8] Norio Asou,[9] Bindya Jacob,[10] Motomi Osato,[10] David N. Haylock,[11] Susan K. Nilsson,[11] Richard J. D'Andrea,[2] Angel F. Lopez,[3] and Mark A. Guthridge[1,7]

[1]Cell Growth and Differentiation Laboratory, Division of Human Immunology, [2]Department of Haematology, [3]Cytokine Receptor Laboratory, Division of Human Immunology, Centre for Cancer Biology, Adelaide, Australia; [4]Department of Mathematics, University of Adelaide, Adelaide, Australia; [5]Department of Haematology and Medical Oncology, Peter MacCallum Cancer Centre, East Melbourne, Australia; [6]Cytokine Signaling Laboratory, Division of Human Immunology, Centre for Cancer Biology, Adelaide, Australia; [7]Department of Medicine, University of Adelaide, Adelaide, Australia; [8]Division of Bioinformatics, The Walter and Eliza Hall Institute of Medical Research, Parkville, Australia; [9]Department of Hematology, Kumamoto University School of Medicine, Kumamoto, Japan; [10]Cancer Science Institute of Singapore, National University of Singapore, Singapore; and [11]Australian Stem Cell Centre, Monash University, Clayton, Australia

Deregulated cell survival programs are a classic hallmark of cancer. We have previously identified a serine residue (Ser585) in the βc subunit of the granulocyte-macrophage colony-stimulating factor receptor that selectively and independently promotes cell survival. We now show that Ser585 phosphorylation is constitutive in 20 (87%) of 23 acute myeloid leukemia (AML) patient samples, indicating that this survival-only pathway is frequently deregulated in leukemia. We performed a global expression screen to identify gene targets of this survival pathway and report a 138-gene βc Ser585-regulated transcriptome. Pathway analysis defines a gene network enriched for PI3-kinase target genes and a cluster of genes involved in cancer and cell survival. We show that one such gene, osteopontin (*OPN*), is a functionally relevant target of the Ser585-survival pathway as shown by siRNA-mediated knockdown of *OPN* expression that induces cell death in both AML blasts and $CD34^+CD38^-CD123^+$ leukemic progenitors. Increased expression of *OPN* at diagnosis is associated with poor prognosis with multivariate analysis indicating that it is an independent predictor of overall patient survival in normal karyotype AML ($n = 60$; HR = 2.2; $P = .01$). These results delineate a novel cytokine-regulated Ser585/PI3-kinase signaling network that is deregulated in AML and identify *OPN* as a potential prognostic and therapeutic target. (Blood. 2009;114:4859-4870)

Introduction

Many hemopoietic cytokines are potent regulators of both cell survival and proliferation. However, although cell survival and proliferation are often viewed as inextricably linked and overlapping cellular fates, they are subject to independent regulation and can be controlled by distinct signaling pathways.[1] For example, cytokines such as granulocyte-macrophage colony-stimulating factor (GM-CSF) and interleukin-3 (IL-3) have been long recognized to promote cell survival in the absence of other biologic responses such as proliferation, differentiation, or activation.[2] This ability to regulate cell survival alone is particularly important in the hemopoietic compartment where many cell types require the continuous presence of cytokines to survive and rapidly execute apoptosis programs on cytokine withdrawal.[3] The corollary of this is that cells receiving a mitogenic signal in the absence of a concomitant growth factor–mediated prosurvival signal attempt to undergo cell-cycle progression but die by apoptosis.[4] Segregating the cytokine-mediated signals that promote hemopoietic cell survival from those that regulate proliferation has important biologic advantages in that it enforces at least 2 obligate steps for cellular transformation and leukemogenesis: one in which deregulated cell proliferation programs are activated and the other in which deregulated survival signals override cell death programs.

Mutations that result in the activation of components of cytokine signaling pathways have been identified in a wide range of human leukemias. These mutations have been found in tyrosine kinase receptors (eg, FLT3-ITD, FLT3-D835, c-KIT–D816, c-KIT–ITD), tyrosine kinases (BCR-ABL, TEL-JAK2), and other components of cytokine signaling pathways (N-RAS, K-RAS).[5] Others have shown that the expression of activating mutants of the GM-CSF and IL-3 receptor β subunit (βc) or deregulation of GM-CSF signaling pathways can promote myeloproliferative disease or leukemia in mice,[6] and loss of the neurofibromatosis type 1 gene results in hypersensitivity to GM-CSF and juvenile chronic myelogenous leukemia.[7] Furthermore, deregulation of phosphoinositide 3-kinase (PI3-kinase) signaling has been observed in a range of cancers, including myeloproliferative diseases and leukemia.[8,9] Collectively, what these findings show is that subverting the normal cytokine receptor signaling pathways promotes deregulated cell survival and proliferation leading to cellular transformation.

Although some cytokines are able to regulate cell survival independently of other cellular responses,[2,3] cytokine receptor signaling motifs specifically dedicated to cell survival only have not been identified. Our previous studies identified 2 cytokine receptor pathways leading to cell survival. Those studies identified

Submitted February 10, 2009; accepted September 8, 2009. Prepublished online as *Blood* First Edition paper, October 5, 2009; DOI 10.1182/blood-2009-02-204818.

The online version of this article contains a data supplement.

The publication costs of this article were defrayed in part by page charge payment. Therefore, and solely to indicate this fact, this article is hereby marked "advertisement" in accordance with 18 USC section 1734.

a specific motif in the cytoplasmic domain of the βc subunit of the GM-CSF receptor composed of Ser585 and Tyr577 that functions as a phospho-binary switch whereby Ser585 phosphorylation specifically regulates cell survival only, whereas Tyr577 phosphorylation integrates both cell survival and proliferation.[10-12] To better define the survival response initiated by Ser585 of βc, we have performed microarray analysis and identified a 138-gene transcriptome of which a major component consists of PI3-kinase target genes. We have previously shown in preliminary studies that the phospho-Tyr577/phospho-Ser585 binary switch may be subject to deregulation in at least some patients with acute myeloid leukemia (AML).[12] We now show that the Ser585 survival-only "arm" of the binary switch is deregulated in 20 (87%) of 23 AML samples, and bioinformatics analysis identifies a Ser585/PI3-kinase gene network. Although the expression level of one Ser585-regulated gene, osteopontin (*OPN*; aka *SPP1*, secreted phosphoprotein 1) correlated with overall survival (OS) in a heterogeneous cohort of 52 AML samples, it was not deemed significant by multivariate analysis. Importantly, however, high *OPN* expression was an independent predictor of poor OS in a 60-patient cohort of cytogenetically normal patients. Furthermore, blockade of *OPN* expression induces cell death in AML blasts as well as leukemic stem and progenitor cells (LSPCs). Our findings define a novel cytokine receptor survival-only pathway that is deregulated in AML and highlight *OPN* as a valuable drug target and prognostic indicator in AML.

Methods

Microarray analysis, pathway analysis, mutational analysis, quantitative RT-PCR, and statistical analysis

Detailed descriptions of the methods for the microarray analysis, pathway analysis, mutational analysis, quantitative reverse transcription–polymerase chain reaction (RT-PCR), and statistical analysis are given in the supplemental Materials (available on the *Blood* website; see the Supplemental Materials link at the top of the online article). All microarray data have been deposited in the Gene Expression Omnibus public database under accession no. GSE18222.

Patient material

Apheresis product and bone marrow or peripheral blood samples were obtained from patients with AML. For the *OPN* expression studies, bone marrow aspirates of 95 consecutive patients diagnosed with AML between 1998 and 2008 at Royal Adelaide Hospital (RAH) Australia were obtained after informed consent according to institutional guidelines in keeping with the Declaration of Helsinki, and studies were approved by the RAH Human Ethics Committee (patient data in supplemental Table 1). Diagnosis was confirmed by using cytomorphology, cytogenetics, and leukocyte antigen expression and was evaluated according to the French-American-British (FAB) classification. Cytogenetic risk classification categories were defined according to the Medical Research Council schema.[13] Patients were treated with standard induction chemotherapy (combination of cytarabine, idarubicin, etoposide) according to the Australian Leukemia Lymphoma Group M7 protocol.[14] For *OPN* expression studies of normal karyotype AML, an additional collection of 35 normal karyotype AML patient bone marrow aspirates were collected from the Kumamoto University School of Medicine, Japan, between 1987 and 2003 after informed consent based on the revised Helsinki protocol and approval by the institutional review board of Kumamoto University School of Medicine, Japan. Samples were analyzed by RT-PCR at the National University of Singapore. All evaluable patients underwent induction and consolidation chemotherapy according to the Japan Adult Leukemia Study Group protocols AML87[15] and AML97[16] and had confirmed normal karyotype by the G-banding method examining 20 mitoses. In cases showing normal karyotype, the absence of fusion mRNAs for RUNX1-ETO or PEBP2β-MYH11 were further confirmed with the RT-PCR method.

Cytokine signaling

Mononuclear cells (MNCs) from healthy donors and patients with AML were isolated by Ficoll-Hypaque density-gradient centrifugation, washed, and resuspended in PBS containing 0.1% human albumin (CSL), and stimulated for 5 minutes with GM-CSF. MNCs were lysed, and the βc subunit was immunoprecipitated with 1C1 and 8E4 anti-βc mAb and subjected to sodium dodecyl sulfate–polyacrylamide gel electrophoresis (SDS-PAGE) and immunoblot analysis.[12] OPN was isolated from human milk, and thrombin was cleaved as previously described.[17,18] Anti–active-ERK pAb (Promega) was used at 50 ng/mL. Anti–phosphorylated Ser473 Akt pAb (Cell Signaling Technology Inc) and anti-p85 pAb (UBI) were used at 1:1000. Affinity-purified phospho-specific anti-β_c phospho-585 pAb, anti-β_c phospho-577 pAb, and anti-14-3-3 pAb were used at 1:1000.[12] PI3-kinase assays were performed as previously described.[10]

Cell survival assays

$CD34^+$ cells were purified from AML MNCs using CD34 MicroBeads according to the manufacturer's instructions (Miltenyi Inc). $CD34^+$ cells were transfected with 50nM BLOCK-iT fluorescent oligo and 50 to 150nM of either GC-control siRNA or scrambled *OPN* siRNA or *OPN* siRNA (Invitrogen; siRNA oligonucleotide sequences are presented in supplemental Table 2). Survival was determined by annexin V–Alexa 568 staining (Roche). Viable cell number was assessed with the use of Flow-Count Fluorospheres (BD Biosciences).

Patient characteristics

All patient characteristics and *OPN* expression levels are presented in supplemental Table 1.

Results

Phospho-Ser585 survival signaling regulates a gene transcriptional program

Our previous studies that used the factor-dependent CTL-EN hemopoietic cell line have shown that the phosphorylation of Ser585 in the cytoplasmic tail of the GM-CSF and IL-3 receptor βc subunit is essential for the binding of the 14-3-3 scaffolding proteins, the recruitment and activation of PI3-kinase, and the specific regulation of hematopoietic cell survival.[10-12] We have now used this CTL-EN model system to interrogate transcriptional targets of Ser585 signaling by microarray screening (Figure 1A).

Data from the National Institute of Aging (NIA) 15K cDNA and Adelaide Microarray Facility (AMF) 21K oligonucleotide microarrays identified 138 genes of which 76 were common to both arrays (supplemental Table 3). Bayesian analysis for the identification of differentially regulated genes was performed on both datasets, and the results from the NIA 15K cDNA arrays are shown (Figure 1B-C). The fold change (M) in response to GM-CSF shows a restricted subset of genes lie off the diagonal, indicating differential response (Figure 1D-E), which included osteopontin (*Opn*), cyclin-dependent kinase 8 (*Cdk8*), vaccinia-related kinase 1 (*Vrk1*), and protein tyrosine phosphatase receptor type S (*Ptprs*). High-ranked genes selected by Gene Ontogeny (GO) analysis (see Figure 2) as having potential roles in cell survival or cytokine signaling are indicated in Figure 1B through E, and the microarray expression profiles for these genes are shown in Figure 1F. A heat map was generated for the 138 genes and shows that Ser585 signaling

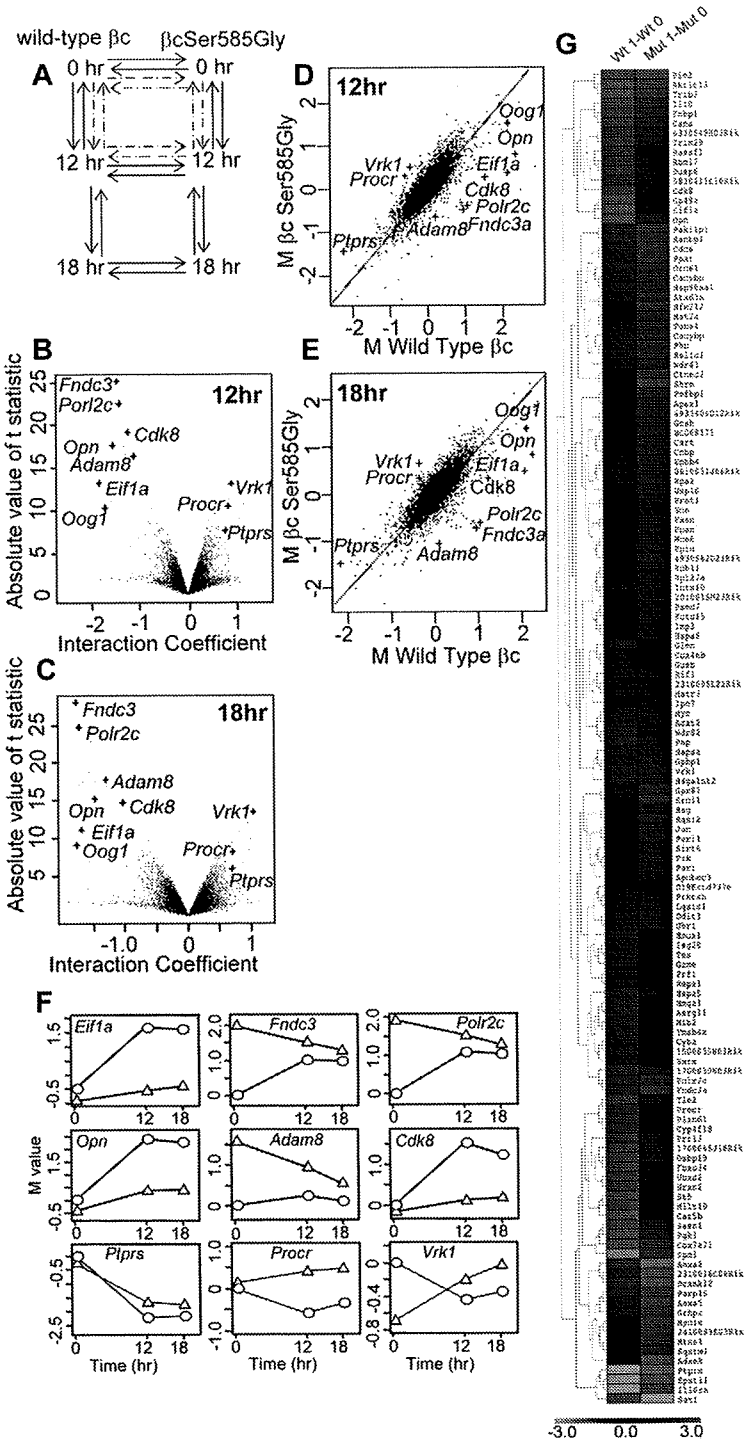

Figure 1. Microarray analysis of the Ser585-survival pathway. CTL-EN cells expressing either wild-type βc or the βcSer585Gly mutant were factor deprived for 18 hours and then stimulated with GM-CSF for 0, 12, and 18 hours. Total RNA was isolated, reverse transcribed, and labeled; cDNA was used to probe either NIA 15k cDNA or AMF 21K microarrays. Pairwise comparisons were performed as in panel A whereby each solid arrow represents a separate 15k cDNA slide (n = 14) and each dotted arrow represents a 21k oligonucleotide slide (n = 8) in which differential gene expression was examined in either (1) cells expressing the wild-type βc or the βcSer585Gly mutant at a single time point or (2) a single cell line at different time points. Microarray data were subjected to Bayesian analysis to identify genes that were differentially expressed in CTL-EN cells expressing the wild-type βc and βcSer585Gly mutant in response to GM-CSF at 12 hours (B) and 18 hours (C). Bayesian analysis is shown whereby the probability that a particular gene is differentially expressed (*t* statistic) is plotted against the magnitude ($\log_2$ scale) of the differential expression (interaction coefficient) for each gene represented on the cDNA array. Negative interaction coefficients correspond to genes that are more strongly expressed in cells expressing the wild-type βc than the βcSer585Gly mutant (eg, genes that are induced by GM-CSF in cells expressing the wild-type βc and not in the βcSer585Gly mutant). Positive interaction coefficients correspond to genes that are more strongly expressed in cells expressing the βcSer585Gly mutant than the wild-type βc (eg, genes that are repressed by GM-CSF in cells expressing the wild-type βc and not in the βcSer585Gly mutant). Selected genes identified by GO analysis in Figure 3 as having a role in cell survival or cytokine signaling and that also showed differential expression are highlighted. (D-E) Microarray data presented as the response in wild-type βc cells (M = $\log_2$ [fold change in response to GM-CSF in CTL-EN cells expressing the wild-type βc]) plotted against the response in the βcSer585Gly mutant cells (M = $\log_2$ [fold change in response to GM-CSF in CTL-EN cells expressing the βcSer585Gly mutant]). Although most genes are either not GM-CSF regulated (M values close to 0 for both wild-type βc and βcSer585Gly mutant) or are GM-CSF regulated in an equivalent manner in cells expressing the wild-type βc and βcSer585Gly mutant (M values lie close to the diagonal line), a restricted subset lies off the diagonal. The M values for the genes highlighted in panels B to E at 0, 12, and 18 hours were plotted for cells expressing either the wild-type βc (○) or the βcSer585Gly mutant (Δ) (F). (G) A clustered heat map of the 138 genes identified as being differentially expressed between the wild-type βc and βcSer585Gly mutant CTL-EN cells in response to GM-CSF was generated with the use of a Euclidean matrix. The M value ($\log_2$ fold change) for both CTL-EN cells expressing the wild-type βc or the βcSer585Gly mutant was converted to a color scale with red indicating that the gene is induced by GM-CSF, green indicating that the gene is repressed, and the color intensity indicating the magnitude of regulation.

regulates a complex gene program consisting of multiple clusters (Figure 1G).

Genes were then selected for further validation by Northern analysis based on their Lod-odds ranking in microarray analysis (Figure 1; supplemental Table 3), GO analysis, Connectivity mapping, and Ingenuity Pathway Analysis (IPA; Figure 3). Although GM-CSF was able to induce the expression of *Opn*, eukaryotic translation initiation factor 1A (*Eif1a*), oogenesin 1 (*Oog1*), and *Cdk8* in CTL-EN cells expressing the wild-type βc, this induction was reduced in cells expressing the βcSer585Gly mutant (Figure 2A-B). In contrast, although *Ptprs* expression was repressed by GM-CSF stimulation of CTL-EN cells expressing the wild-type βc, this repression was reduced in cells expressing the βcSer585Gly mutant (Figure 2A-B).

Phospho-Ser585 survival-only pathway regulates a PI3-kinase signaling network

GO analysis indicated that more than half of the 138 genes identified perform functions related to cytokines and signal transduction (29%) and transcription and translation (24%; Figure 3A; supplemental Table 3). The Ser585 gene program was examined in silico with the Connectivity Map to identify potential associations with transcriptional signatures from drug/compound treatments.[19]

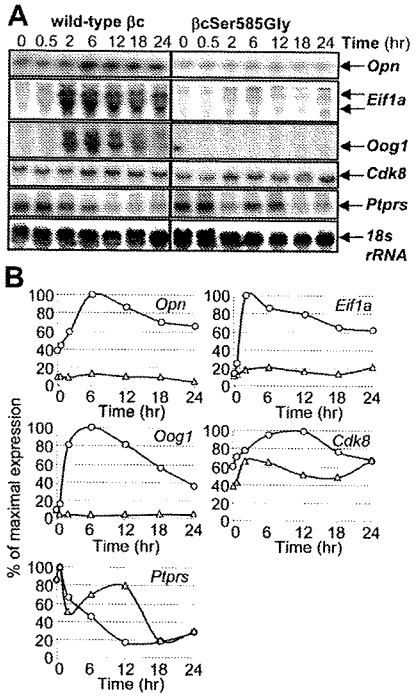

Figure 2. Ser585 regulates the expression of specific genes. CTL-EN cells expressing either the wild-type βc or the βcSer585Gly mutant were stimulated with GM-CSF for the indicated times after which time total RNA was purified and subjected to Northern analysis by using ^{32}P-labeled cDNA probes (A). The Northern blot signals for each gene in CTL-EN cells expressing the wild-type βc (○) and βcSer585Gly mutant (Δ) were quantified by ImageQuant analysis from PhosphorImager screens and plotted as a percentage of the maximum signal observed (B).

This analysis identified a significant association between the 138 genes identified in our studies and the gene signatures produced by the PI3-kinase inhibitor, LY294002, in 13 of 17 microarray experiments across diverse cell types (Figure 3B red bar; connectivity score, −0.408; $P = .009$). As shown in Figure 3C, Ser585-regulated genes (blue lines) cocluster with top-ranked LY294002-sensitive genes (red region), and the frequency of Ser585-regulated genes (probe frequency) significantly increases over a random distribution (dotted line) as the Lod-ranking of LY294002-regulated genes increases (Figure 3C; $P < .001$, Wilcoxon rank sum test). Of the 138 genes identified in our screen, 53 (38%) correspond to LY294002-sensitive genes and are highlighted by the gray shading in Figure 3C as well as in supplemental Table 3. To further examine this Ser585/PI3-kinase network, we used IPA to identify biologic networks associated with known functional, biochemical, and disease interactions. This analysis showed a significant association with cancer (27 of 53, 51%) and cell death (24 of 53, 45%; Figure 3D) and identified a highly integrated Ser585/PI3-kinase signaling network (Figure 3E).

Phospho-Ser585 survival signaling is deregulated in AML

Previous preliminary studies raised the possibility that Ser585 phosphorylation could be deregulated in at least some patients with AML.[12] Given that the IPA showed a significant association of Ser585-regulated genes with cancer and cell death (Figure 3D), we performed an investigation of the regulation of Ser585 phosphorylation in a panel of 23 AML patient samples. It was not possible to obtain sufficient numbers of normal CD34$^+$ cells from bone marrow donors to examine the regulation of Ser585 phosphorylation with our phospho-specific antibodies. Furthermore, CD34$^+$ progenitors respond poorly to GM-CSF, most probably because of the low levels of GM-CSF receptor expression (data not shown). We therefore examined the Ser585 phosphorylation profile of primary MNCs because these cells have been previously shown to robustly respond to GM-CSF.[12] Consistent with these previous findings, Ser585 and Tyr577 phosphorylation in MNCs derived from peripheral blood of healthy donors occurred in a biphasic manner with maximal Ser585 phosphorylation occurring at approximately 1pM and decreased Ser585 phosphorylation occurring at approximately 1000pM (Figure 4A). Quantification of Western blot analysis and unsupervised cluster analysis indicated that Ser585 was constitutively phosphorylated in 20 (87%) of 23 AML patient samples ($P < .05$, Mann-Whitney U test). AML38, AML96, and AML97 did not show statistically significant constitutive Ser585 phosphorylation (Figure 4C). In contrast, Tyr577 phosphorylation remained ligand dependent in 17 (94%) of 18 AML samples, occurring at approximately 1000pM (Figure 4C). Deregulated Ser585 phosphorylation in AML was evidenced as (1) increased basal Ser585 phosphorylation in the absence of GM-CSF (0pM) and (2) a failure to down-regulate Ser585 phosphorylation in response to 1000pM GM-CSF. Importantly, our results show that constitutive Ser585 phosphorylation was observed across diverse FAB and cytogenetic classifications (Figure 4C), indicating that constitutive Ser585 survival signaling is a common event in AML.

We then sought to examine the Ser585/PI3-kinase gene network identified in Figure 3 by determining the mRNA expression of specific genes in AML samples. For these experiments, we used both purified bone marrow–derived CD34$^+$ progenitor cells and mature CD14$^+$ monocytes as healthy donor controls. Our results show that *BCL2*, *VRK1*, *POLR2C*, *CDK8*, *FNDC3*, and *PTPRS* were more highly expressed in bone marrow CD34$^+$ cells from healthy donors and became down-regulated in mature CD14$^+$ monocytes (Figure 4D). Consistent with their immature phenotype, these genes (with the exception of *PTPRS*) were also highly expressed in AML blasts compared with CD14$^+$ monocytes (Figure 4D). Thus, the genes identified in our screen for Ser585 targets are more strongly expressed in primitive CD34$^+$ populations from both healthy donors and patients with AML. Attempts to disrupt the expression of Ser585-regulated genes by siRNA-mediated knockdown of βc expression were not successful despite obtaining high-transfection efficiencies (62%-74%) and using 7 different siRNAs obtained from 2 different companies (data not shown). The lack of significant βc knockdown may have been related to several factors, including the stability or transcriptional rates for βc mRNA. Interestingly, we noted that, although most Ser585-regulated genes in Figure 4D showed a narrow range of expression in AML, *OPN* was distinct in that it displayed a broad range of expression. Furthermore, pairs plots analysis (supplemental Figure 1) indicated that *OPN* expression was independently regulated with respect to all other genes analyzed in Figure 4D, suggesting that, although *OPN* was identified as a Ser585-regulated gene (Figures 1-2), other pathways also affect *OPN* expression in AML.

Deregulation of the phospho-Ser585/PI3-kinase signaling pathway and the regulation of *OPN* expression in AML

In line with the constitutive Ser585 phosphorylation observed in AML (Figure 4), we also found constitutive recruitment of both 14-3-3 and the p85 subunit of PI3-kinase to βc and deregulated PI3-kinase activity (Figure 5A-C). Tamburini et al[20] have shown that the activation status of the PI3-kinase signaling pathway is a prognostic indicator of OS in AML. We therefore examined

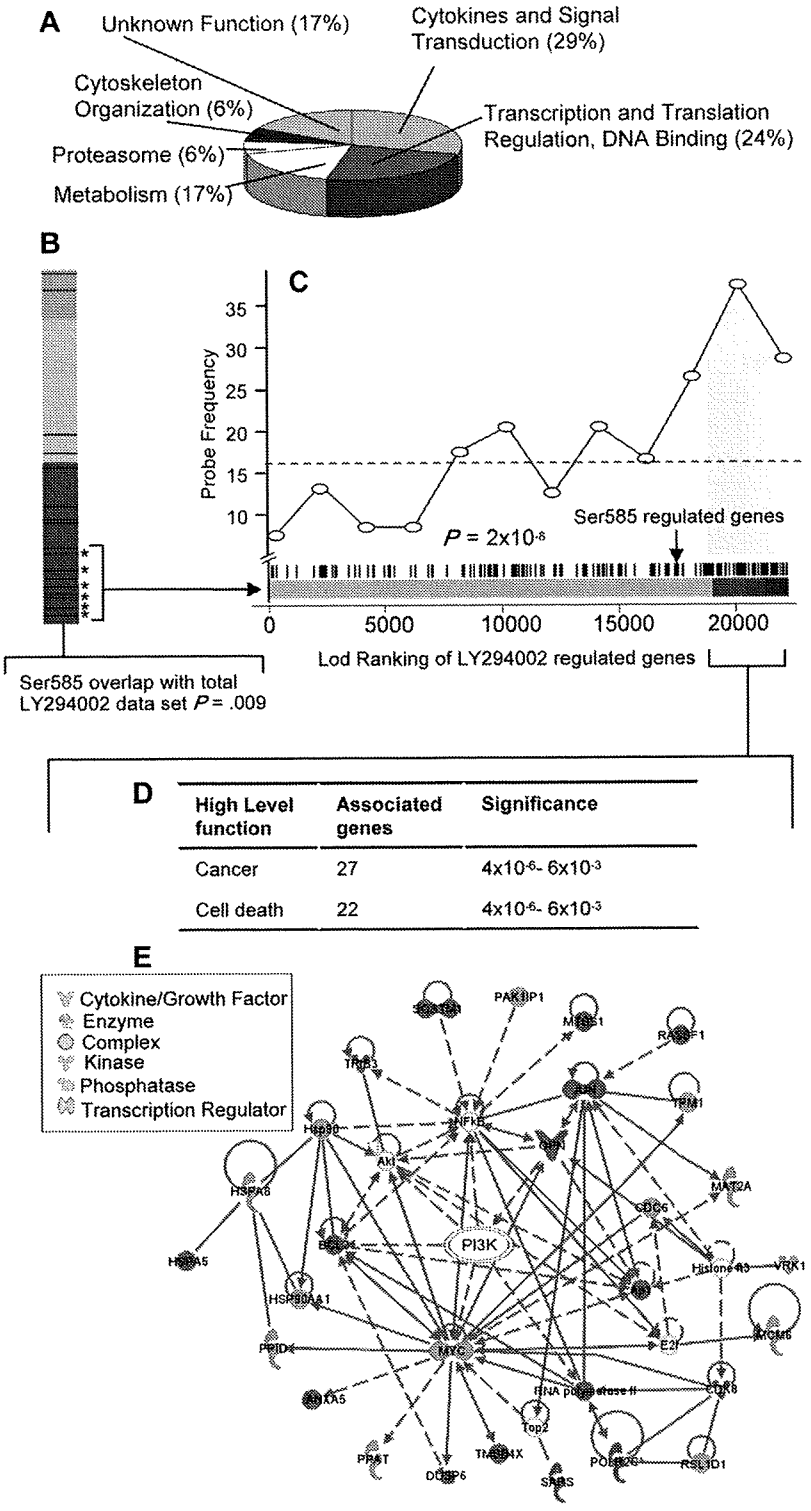

High Level function	Associated genes	Significance
Cancer	27	$4x10^{-6}$- $6x10^{-3}$
Cell death	22	$4x10^{-6}$- $6x10^{-3}$

Figure 3. Identification of a Ser585/PI3-kinase transcriptional network. (A) Gene ontology (GO) (www.geneontology.org/) classifications are shown for the 138 Ser585-regulated genes identified by microarray screening. (B) Connectivity mapping[19] of the 138 Ser585-regulated genes indicated negative connectivity with the expression change induced by the PI3-kinase inhibitor, LY294002. A negative connectivity (red) represents genes that are either induced by Ser585 and repressed by LY294002 or repressed by Ser585 and induced by LY294002. All 453 experiments in the Connectivity Map database were ranked by their connectivity score with the 138 Ser585-regulated genes identified in our studies. Each of the LY294002 comparisons (n = 17) is highlighted as a black bar on the heat map, and colors represent a negative (red), no connection (gray), or positive connection (green) between the 138 Ser585-regulated genes identified in our studies and individual LY294002-induced gene expression changes for each array in the Connectivity Map database. A cluster of LY294002 experiments (13 of 17) lie within the red region, indicating a statistically significant enrichment of our 138 Ser585-regulated genes and the LY294002 differentially expressed genes ($P = .009$). (C) Analysis of the overlap between the 138 Ser585-regulated gene set identified in our studies and the LY294002-sensitive genes in the Connectivity database. We pooled the data from the 6 top-ranked MCF7 cell LY294002 microarrays that showed significant overlap with our 138 gene set (bracketed asterisks) and performed a Wilcoxon rank sum test to compare a ranked list of LY294002 sensitive genes (Lod-ranking of LY294002-regulated genes) with our 138 gene set. Each blue line corresponds to an individual probe identified from our screen. Ser585-regulated genes (blue lines) cluster with top-ranked LY294002-sensitive genes (red region). Plotting this overlap shows a significant enrichment above a random distribution (dotted line) in Ser585-regulated genes (probe frequency) as the Lod-ranking of LY294002-regulated genes increases ($P < .001$). Of the 138 genes identified in our screen, 53 (38%) correspond to LY294002-sensitive genes encompassed by the gray portion of the graph (LY294002 cutoff; $P = .01$). (D) The 53 Ser585/PI3-kinase–regulated genes identified in panel C together with their fold change were uploaded into the IPA and overlaid onto a global molecular network developed from information contained in the Ingenuity Pathways Knowledge Base. Networks of genes were then algorithmically generated based on their connectivity to known functional, biochemical, and disease interactions. A significant overlap with genes involved in cancer and cell death was observed ($P < .001$, right-tailed Fisher exact test). (E) The 53 Ser585/PI3-kinase–regulated genes identified in panel C were subjected to IPA mapping of network interactions. This analysis showed that 27 of 53 genes constitute a gene network with red denoting Ser585-induced genes and green denoting Ser585-repressed genes. Node shape denotes the indicated gene function or biologic process.

PI3-kinase and Ras-MAP-kinase signaling by examining the phosphorylation of Akt and ERK, respectively. We observed elevated basal Akt phosphorylation in 12 of 13 AML patient samples (Figure 5D), whereas elevated ERK phosphorylation was observed in 5 of 11 patient samples (Figure 5E). It is important to note that, although both Ser585 (Figure 4C) and Akt (Figure 5D) phosphorylation were both deregulated in most AML patient samples, a broad range of *OPN* expression (Figure 4D) was observed. Statistical analysis comparing *OPN* expression (high vs low) and basal Akt phosphorylation levels (high vs low) in 11 AML samples from Figure 5D was not significant ($P = .3$, χ^2 test), indicating that elevated Akt phosphorylation does not directly correlate with increased expression of *OPN*. However, to examine the possibility that PI3-kinase signaling can promote *OPN* expression, we examined the effect of LY294002 and wortmannin treatment on *OPN* expression. Blockade of PI3-kinase signaling in 2 AML samples exhibiting high basal Akt phosphorylation resulted in a significant decrease in *OPN* mRNA expression (Figure 5F;

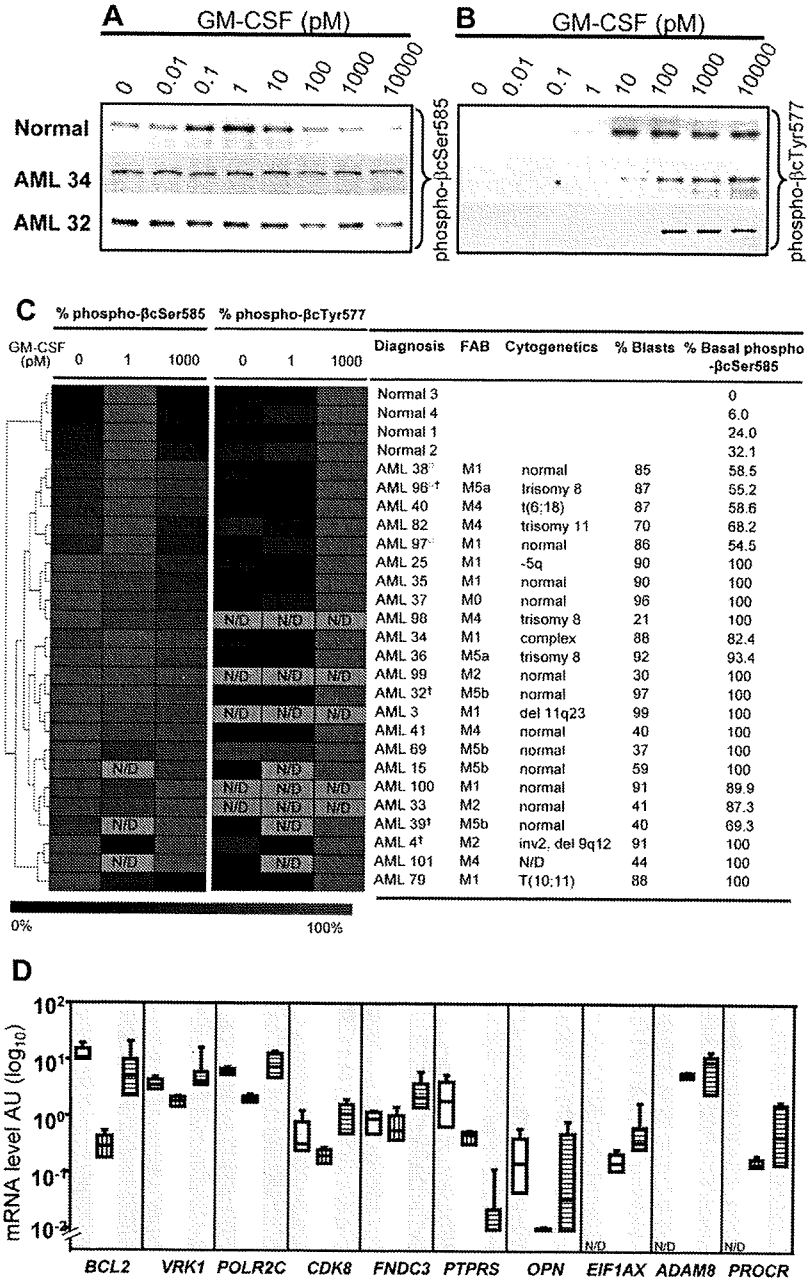

Figure 4. Ser585 phosphorylation is selectively deregulated in AML. MNCs from either healthy donors or patients with AML were stimulated with the indicated concentrations of GM-CSF for 5 minutes. The cells were then lysed, and βc was immunoprecipitated with βc-specific mAbs. Immunoprecipitates were subjected to SDS-PAGE and immunoblotted with affinity-purified phospho-specific anti–phospho-βcSer585 and anti–phospho-βcTyr577 antibodies. Typical results for a healthy donor and 2 AML samples are shown in panel A and panel B. The Western blot results from GM-CSF dose-response experiments on healthy donors (n = 4) and patients with AML (n = 23) were quantified by laser densitometry, and the quantified signals were converted to a heat map with the use of MeV (www.tm4.org/mev.html), where the intensity of red indicates the magnitude (%) of phosphorylation; gray, samples not done (ND); □, patients who did not show statistically significant constitutive Ser585 phosphorylation; †, samples derived from relapsed patients. Hierarchical cluster analysis was performed for Ser585 phosphorylation signals by using a Euclidean matrix with complete linkage, and the resultant heat maps are shown (C). FAB classifications, cytogenetics, blast count, and percentage of basal phosphorylation of βcSer585 for each AML are indicated alongside the heat maps. (D) Quantitative RT-PCR for the indicated genes was performed on total RNA extracted from purified bone marrow–derived CD34$^+$ progenitor cells (n = 4; open boxes), mature CD14$^+$ monocytes (n = 4; vertical striped boxes), and AML MNCs (n = 10; AML32-41, horizontal striped boxes). Boxes represent the interquartile range that contains 50% of the values, the horizontal lines mark the median, and the error bars indicate the SD. Data are normalized to β-actin expression and are presented as relative mRNA expression ($\log_{10}$). N/D denotes quantitative RT-PCR not done in bone marrow–derived CD34$^+$ progenitor cells.

$P < .01$). We next examined the possibility that OPN may also act upstream and activate PI3-kinase signaling and Akt phosphorylation. For these experiments we used the factor-dependent TF.1 erythroleukemia cell line because it exhibits low levels of basal Akt phosphorylation. Opn stimulation was not able to induce significant Akt phosphorylation, whereas clear Akt phosphorylation was detectable in response to GM-CSF (supplemental Figure 2). Together, these results suggest that, although PI3-kinase in AML can contribute to *OPN* expression, other pathways are also probably involved.

Targeting OPN blocks the survival of AML blasts and LSPCs

Of the genes identified in the Ser585/PI3-kinase gene network, several are known regulators of cell survival, including *BCL2*,[21] *CDK8*,[22] *PTPRS*,[22] and *OPN*.[23,24] However, *OPN* was unique in that it is a secreted protein and would be biologically accessible for therapeutic antagonists such as mAbs. In addition, *OPN* exhibited a high probability of differential regulation by Ser585 (supplemental Table 3), was validated by Northern blot (Figure 2), and was predicted by IPA to directly link with PI3-kinase, a known canonical survival-signaling hub (Figure 3E). We therefore addressed the possibility that *OPN* could function as a survival factor in AML by siRNA-mediated knockdown in CD34$^+$ blasts. Compared with either a GC-control or scrambled control siRNAs, siRNA-mediated *OPN* knockdown resulted in a 58% decrease in *OPN* expression with no off-target effects observed for either *BCL2* expression (Figure 6A) or actin (data not shown). Furthermore, siRNA-mediated *OPN* knockdown resulted in a significant reduction in cell survival (Figure 6A; $P = .02$). Similarly, 50nM of siRNA complexes also resulted in significant reduction in cell survival, suggesting minimal cytotoxicity (supplemental Figure 3). In addition, 4 of 5 AML patient samples exhibiting high *OPN* expression showed increased cell death after *OPN* siRNA knockdown (Figure 6B AML4, AML32, AML35, AML36; $P < .05$),

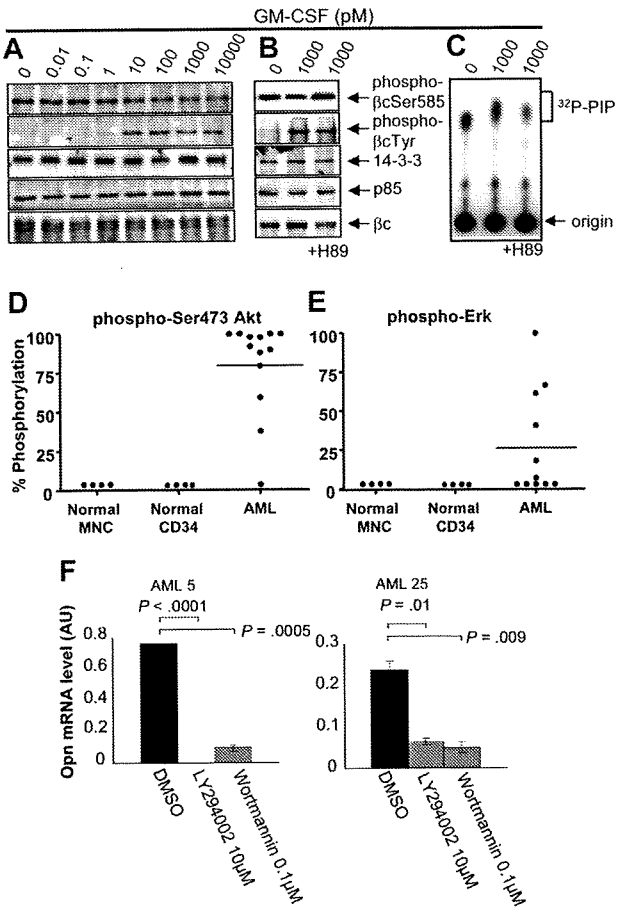

Figure 5. AML blasts exhibiting constitutive Ser585 phosphorylation also show deregulated PI3-kinase signaling. Mononuclear cells from patients with AML (A, AML37; B-C, AML101) were stimulated with the indicated concentrations of GM-CSF for 5 minutes. Where indicated, cells were preincubated for 1 hour with 10μM H89 or DMSO vehicle control before GM-CSF stimulation. Cells were then lysed and βc immunoprecipitated and subjected to SDS-PAGE and immunoblot analysis with the indicated antibodies. (C) In vitro kinase assay for PI3-kinase activity was performed on βc immunoprecipitates with phosphatidyl inositol 4,5 phosphate (PIP) and ^{32}P-γ-ATP as described in "Cytokine signaling." ^{32}P-PIP and the origin are indicated (C). Whole-cell lysates were blotted with anti–phospho-Ser473Akt (D) or anti–phospho-ERK (E), and signals were quantified by laser densitometry. The level of phosphorylation in the absence of GM-CSF was plotted as a percentage of maximum signal observed after GM-CSF stimulation. (F) Purified CD34$^+$ cells from the indicated AML patient samples were treated with 10μM LY294002 or 0.1μM Wortmannin or DMSO for 24 to 72 hours in IMDM medium containing 0.5% FCS, after which time viable cell number was assessed with Flow-Count Fluorospheres, and total RNA was isolated for *OPN* quantitative RT-PCR as described in Figure 4D.

whereas no significant induction of cell death was observed in an AML patient sample with undetectable levels of *OPN* expression (Figure 6B AML37). It is important to note that 100% of patient samples analyzed in Figure 6A and B coexpressed CD34 and CD33, with CD33$^+$ cells in these samples ranging between 65% and 98%. These findings are consistent with previous reports showing that more than 85% of patients have AML CD34$^+$ blast cells coexpressing significant levels of CD33.[25] Because LSPCs are central to the long-term maintenance and growth of AML, we then sought to examine the effect of *OPN* expression knockdown on the survival of this clinically relevant target cell population. The CD34$^+$/CD38$^-$/CD123$^+$ fraction has been shown to contain the self-renewing, tumor-initiating population of LSPCs.[26,27] Opn knockdown in purified CD34$^+$/CD38$^-$/CD123$^+$ LSPCs (Figure 6C) resulted in a significant decrease in cell survival in vitro in 4 of 4 patient samples compared with both GC-control siRNA and scrambled control siRNA (Figure 6D; $P < .05$). No evidence of cytotoxicity by either the scrambled siRNA control or siRNA concentration (50nM vs 150nM) was observed (Figure 6D). Quantitative RT-PCR confirmed knockdown of *OPN* expression in LSPCs (supplemental Figure 4). Our results would suggest that knockdown of *OPN* expression results in cell death of AML blasts and LSPCs, indicating that *OPN* can support cell survival. Although OPN has not previously been shown to act as a mitogen for hemopoietic cells, we do not exclude the possibility that *OPN* expression in AML may also promote deregulated proliferation.

OPN is a prognostic indicator of OS in AML

Given the role of *OPN* in promoting the survival of AML blasts and LSPCs, we considered the possibility that *OPN* expression levels may have prognostic significance. We quantified *OPN* mRNA expression in an expanded cohort of 95 consecutive diagnostic AML samples obtained at the RAH (supplemental Table 1). *OPN* expression ranged between 0 and 16 AU (median, 0.23 AU) with detectable expression in 67% of patients (64 of 95) (supplemental Table 1; Figure 7A). There was no striking association between *OPN* expression and FAB classification, although we noted that M3 had higher *OPN* levels compared with M4 ($P < .05$, Dunn post test) or M5 ($P < .05$; Figure 7B). Dividing patients into either low (< 0.23 AU, below median value) or high (> 0.23 AU, above median value) *OPN* expression, we examined OS by Kaplan-Meier estimates and the log-rank test. Of the 95 patients in our cohort, 52 (62%) had received standard induction chemotherapy and were evaluable for analysis. There was no significance difference in age, sex, white blood cell count (WCC), marrow blast percentage, FAB grouping, *FLT3* mutation status, cytogenetic grouping, or allotransplantation numbers between the *OPN*-high and *OPN*-low groups (Table 1). Patients with high *OPN* (median OS, 225 days) showed a significantly reduced OS compared with patients with low *OPN* (median OS, 552 days; Figure 7C; n = 52; HR, 2.09; 95% CI, 1.16-4.22; $P = .02$), suggesting *OPN* expression may have prognostic significance in AML.

The effect of *OPN* expression on patient outcome was further examined by a multivariate Cox proportional hazards model. WCC and cytogenetics remained independent risk factors after multivariate analysis (Table 2; $P < .05$). Controlling for these factors, *OPN* expression was no longer a significant predictor of OS (Table 2; n = 52; $P = .08$), suggesting that variables such as cytogenetic risk classification may be influencing the effect of *OPN* on patient outcome.

Patients with AML with normal cytogenetics falling within the intermediate-risk category remain a difficult group to treat because of their heterogeneous prognosis and response to therapies. We therefore examined the effect of *OPN* expression on OS within cytogenetically normal AML. Although there was a trend toward significance in normal karyotype AML in our RAH dataset ($P = .1$), our sample size was limited (n = 25). We therefore analyzed an expanded collection of 60 patients with normal-karyotype AML who had been previously treated with induction chemotherapy (25 patients from the RAH collection plus 35 patients from Kunamoto, Japan; supplemental Table 1). The range of expression for the RAH samples was 0 to 4.82 AU (median, 0.09 AU), whereas the range for the Kunamoto samples was 0.07 to 32.2 AU (median, 0.67 AU; Figure 7D). Taking an institutional-specific median split to divide patients into high versus low *OPN* expression, we performed Kaplan-Meier log-rank analysis for OS. We noted that, although there was no significance difference in sex, WCC, *FLT3*, *NPM1* mutation status, or transplantation frequency between *OPN*-high and *OPN*-low groups, the *OPN*-high group was